

The structural landscape and diversity of *Pyricularia* *oryzae* MAX effectors revisited

Mounia LAHFA¹, Philippe BARTHE¹, Karine DE GUILLEN¹, Stella CESARI², Mouna RAJI¹, Thomas KROJ², Marie Le Naour--Vernet², François Hoh¹, Pierre GLADIEUX², Christian ROUMESTAND¹, Jérôme GRACY¹, Nathalie DECLERCK¹, André PADILLA^{1*}

¹ Centre de Biologie Structurale, Univ Montpellier, CNRS UMR 5048, INSERM U 1054, Montpellier, France.

² PHIM Plant Health Institute, Univ Montpellier, INRAE, CIRAD, Institut Agro, IRD, Montpellier, France

* Corresponding author

E-mail: andre.padilla@cbs.cnrs.fr

Keywords: *Pyricularia oryzae*, MAX effectors, NMR, protein structure, AlphaFold

Short title: MAX structural family portrait

ABSTRACT

Plant pathogenic fungi secrete a wide variety of small proteins, named effectors. *Magnaporthe* AVR-like (MAX) effectors constitute a superfamily of secreted proteins widely distributed in *Pyricularia* (*syn. Magnaporthe*) *oryzae*, a devastating fungus responsible for blast disease in cereals such as rice. In spite of high evolutionary sequence divergence, MAX effectors share a common fold characterized by a β -sandwich core often stabilized by a conserved disulfide bond. In this study, we investigated the structural landscape and diversity within this effector family based on a previous phylogenetic analysis of *P. oryzae* protein sequences that identified 94 ortholog groups (OG) of putative MAX effectors. Combining protein structure modeling approaches and experimental structure determination, we validated the prediction of the conserved MAX core domain for 77 OG clusters. Four novel MAX effector structures determined by NMR were in remarkably good agreement with AlphaFold2 (AF) predictions. Based on the comparison of the AF-generated 3D models we propose an updated classification of the MAX effectors superfamily in 20 structural groups that highlight variation observed in the canonical MAX fold, disulfide bond patterns and decorating secondary structures in N- and C-terminal extensions. About one-third of the MAX family members remain single, showing no obvious structural relationship with other MAX effectors. Analysis of the surface properties of the AF MAX models also highlights the very high variability remaining within the MAX family when examined at the structural level, probably reflecting the wide diversity of their virulence functions and host targets.

Author summary

MAX effectors are a family of virulence proteins from the plant pathogenic fungus *Pyricularia* (*syn. Magnaporthe*) *oryzae* that share a similar 3D structure despite very low amino-acid sequence identity. Characterizing the function and evolution of these proteins requires a detailed understanding of their structural diversity. We used a combination of experimental structure determination and structural modeling to characterize in detail the MAX effector repertoire of *P. oryzae*. A prediction pipeline based on similarity searches and structural modeling using the AlphaFold2 (AF) software were used to predict MAX effectors in a collection of 120 *P. oryzae* genomes. We then compared AF models with experimentally validated NMR structures. The resulting models and experimental structures revealed that the preserved MAX core coexists with extensive structural variability in terms of structured N- or C-terminal extensions. For each of the AF models, we also analyzed the surfaces of the canonical fold that may be involved in protein-protein interactions. This work constitutes a major step in mapping the functional network of MAX effectors through their structure by identifying possible recognition sites that may help focusing studies of their putative targets in infected plant hosts.

Introduction

Fungal plant pathogens secrete small proteins, called effectors, which promote disease by targeting cellular processes in the host plant. These fungal effectors are usually identified based on their secretion signal and other features such as cysteine enrichment [1,2]. There are hundreds of predicted effectors in the genomes of plant pathogenic fungi and very few of them show sequence similarities and/or homology to known proteins or protein domains. Some effectors are of particular interest since they constitute avirulence (AVR) factors that can be detected by plant immune systems and render crops resistant to severe diseases. Because fungal effectors usually show no amino-acid sequence homology to known proteins or protein domains, their biological function cannot be inferred from systematic *in silico* analysis (such as domain searches) but has so far been elucidated on a case-by-case basis. As a huge and growing number of putative effectors is being discovered, deciphering the functions and adaptive evolution of fungal effectors thus requires robust predictive tools for analyzing protein sequences and identifying candidates on which to prioritize functional and structural studies.

Recently, a combination of primary sequence pattern searches and structural modeling resulted in a major breakthrough in the study of effector biology by revealing that fungal effector repertoires are actually dominated by a limited number of families sharing common structures despite extensive sequence variability [3–5].

One such family is the superfamily of MAX (*Magnaporthe* AVRs and ToxB-like) effectors we identified in *Pyricularia oryzae* (synonym: *Magnaporthe oryzae*), the fungus causing blast disease in rice, wheat, and other cereals or grasses. This pathogenic fungus is both a major threat to global food security and a prime

experimental model in plant pathology because of its ability to rapidly evolve to escape recognition of the plant immune system. By solving the solution structure of two *P. oryzae* effectors, AVR1-CO39 and AVR-Pia, we discovered strong structural similarities between these sequence-unrelated effectors as well as with the ToxB effector from the wheat infecting fungus *Pyrenophora tritici-repentis* [6]. This latter showing sequence homology with a putative effector from *M. oryzae*, we solved the crystal structure of this MoToxB protein (supplementary materials and methods) and confirmed its structural similarity with ToxB as well as with the other structurally determined *P. oryzae* MAX effectors that together with MoToxB share less than 13% sequence identity (S1 Fig). Like other MAX effectors, MoToxB is structured as a 6-stranded β -sandwich (β 1 to β 6) of two triple-stranded β -sheets with a β 6 β 1 β 2- β 3 β 4 β 5 topology. The highly conserved disulfide bond forms a bridge between β 1 and the loop connecting β 4 and β 5 while a second disulfide bond connects β 2 and β 6 (Fig 1).

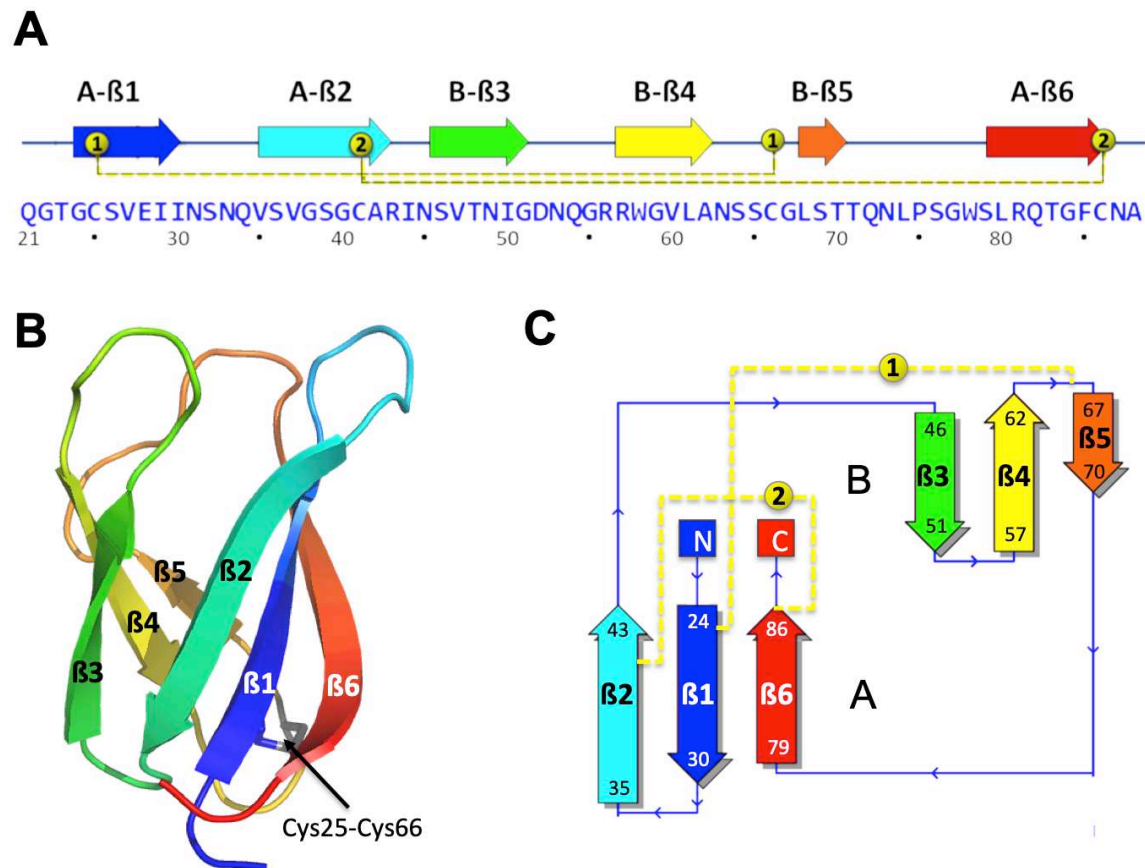


Fig 1. Structure of the *M. oryzae* ToxB (MoToxB) MAX effector

Primary and secondary structure of MoToxB showing the triple-stranded beta-sandwich forming the conserved MAX core with the two beta-sheets labeled by A and B, strands indicated by arrows and two disulfide bonds in yellow dotted lines. Disulfide bond “1” is almost strictly conserved in MAX effectors. (B) Cartoon representation of MoToxB crystal structure (PDB 6R5J) shown in rainbow color and the conserved disulfide bond “1” shown in sticks. (C) MoToxB topology diagram drawn by PDBsum and colored using the same color scheme as in A and B.

MAX effectors are specific to plant pathogenic ascomycetes fungi and they have undergone a major expansion in *P. oryzae*, suggesting an important role in the infection process. Our recent analysis of 120 isolates of *P. oryzae* identified 58 to 78 MAX effector genes per genome, corresponding to 5 to 10% of the full repertoire of predicted effectors. In addition to this genetic expansion, the importance of MAX

effectors in *P. oryzae* virulence is supported by our finding that many MAX effectors are massively expressed during the early stages of plant infection in a host-dependent manner [5–7]. They are also specifically targeted by the plant immune system: nearly half of the cloned avirulence genes of *P. oryzae*, which encode avirulence (AVR) factors recognized by host resistance proteins in blast disease resistant cultivars, correspond to MAX effectors [6,8–11]. Analysis of the recognition of the MAX effectors AVR-Pia, AVR1-CO39, and AVR-Pik by rice immune receptors indicates that they may target a specific class of proteins called small HMAs (sHMAs) [12], which show similarity to copper chaperones containing a heavy metal-associated domain (HMA). Experimental evidence supports this hypothesis in AVR-Pik, but the sHMA proteins' biological function and role in the infection process are unknown. Another MAX effector, AvrPiz-t, targets four different host proteins involved in different cellular processes [13,14].

In our previous study, we have explored the genetic diversity of the MAX effector family in different *P. oryzae* host-specific lineages [7] in order to get insights into the adaptive evolution and the selective forces that shape the molecular variability of structurally analogous effectors. Focusing on the variations observed within the predicted conserved MAX core, we identified a total of ~7800 orthologous and paralogous sequences of putative MAX effectors clustered in 94 orthogroups (OG). Pan-genome analyses showed that the MAX effector repertoire is highly plastic compared to other secreted proteins, both in terms of the presence/absence of orthogroups and the sequence variability within OG clusters. Interestingly, mapping of polymorphic residues for the three effectors whose binding interfaces have been experimentally characterized (AVR1-CO39, AVR-Pia and AVR-Pik) [7] suggests that

amino acid changes often co-localized with residues interacting with immune receptors and, presumably, also with their host target proteins.

In order to further exploit the structure-based repertoire of *P. oryzae* MAX effectors and get a complete view of their molecular diversity, a systematic and robust analysis of their three-dimensional structure, especially outside the MAX core domain, is still needed. Such analysis could allow a more comprehensive classification of effector proteins within the MAX family and provide information on how MAX effectors evolve and adapt to specific hosts. Indeed, many MAX effectors possess N- and C-terminal extensions that could establish specific protein-protein interactions playing a key role in the function of MAX effectors and their interference with different host molecular processes. Examining in more details these extensions, as well as other non-conserved structural features, may thus provide insights into the mechanism by which MAX effectors acquire new virulence capabilities.

In the present study, we combined experimental and computational approaches to finely characterize the structural diversity of MAX effectors. In order to evaluate the reliability of the homology modeling approach we previously used for predicting MAX effectors, we undertook structural studies of several MAX candidates and succeeded in solving four new structures by Nuclear Magnetic Resonance (NMR). Comparison of the new experimental MAX structures with their corresponding 3D models generated by template-based or *ab initio* modeling programs revealed the high accuracy with which AlphaFold2 (AF) can predict the structure of MAX effectors, including for non-conserved side-chains in terminal extensions that were not previously observed. We therefore revisited with the use of AF the structural landscape of *P. oryzae* MAX effectors and validated the presence of a MAX core in 77 of the 94 MAX OG clusters defined in Le Naour--Vernet et al. 2023

[7]. Structural alignment of the AF models allow us to describe the structural consensus and variability within the MAX family, from the canonical fold, but also including disulfide bond pattern variations, decorating secondary structures within the N- and C-terminal extensions that may be involved in protein-protein interactions as well as surface properties, including stickiness and electrostatics of the core domain of MAX effectors.

This work represents the most extensive structural analysis of a fungal effector family of a plant pathogen to date. It also provides valuable knowledge for analyses aimed at elucidating the function of MAX effectors, notably through the prediction of interaction sites within the MAX fold that could contribute to targeting host proteins during infection.

Results

NMR structures validate template-based modeling of MAX effectors

In our previous phylogenic analysis of the MAX effector repertoire in *P. oryzae*, we used a hybrid multiple Template Modeling (TM) strategy for predicting the 3D structure of the conserved MAX core of representative sequences of 94 orthogroups (OG) and we evaluated the reliability of these 3D models (referred as TM-pred models) by calculating the TM-pred score [7]. The TM-pred score is an estimate of the TM-score given by TM-align superimposition [15] that would be observed when structurally aligning the TM-pred model with the corresponding experimentally resolved structure. At the time this analysis was performed with only 8 experimental structures of MAX effectors used as templates for homology modeling in a training data set used to set-up of the TM-pred scoring function [7]. From the online table <https://pat.cbs.cnrs.fr/magmax/model/> (see also Materials and Methods) can be downloaded the TM-pred models and their TM-pred scores calculated for the predicted MAX core of 94 OG proteins (i.e. selected representative sequences of MAX OG clusters, as listed in the S2 Table). Comparison of the TM-pred scores shown in the S1 Fig indicates that ~90% of the OG proteins could be modeled with a MAX structure having a predicted accuracy exceeding a TM-pred score > 0.6, whereas only three TM-pred models of OG proteins (OG22, OG77 and OG85) had a TM-pred score below 0.5 and were rejected as MAX effectors.

In order to assess the validity of these predictions, we aimed to resolve new experimental structures not included in the set of templates used in training the TM-pred score. We attempted to express genes corresponding to mature proteins from 10 OG clusters was attempted (S3 Table) for MAX effector candidates showing high expression level during the biotrophic stage of infection [7]. Using NMR spectroscopy

we successfully determined the structure of four OG cluster representatives (OG28, OG47, OG60 and OG67) and we confirmed that all four proteins are MAX effectors (referred to as “MAX” instead of “OG clusters” from hereon). The 20 best-refined conformers obtained for each of these effectors were superimposed (Fig 2A) and the low root mean square deviations (r.m.s.d) support the high quality of the NMR structures. The complete structural statistics are given in S4 Table.

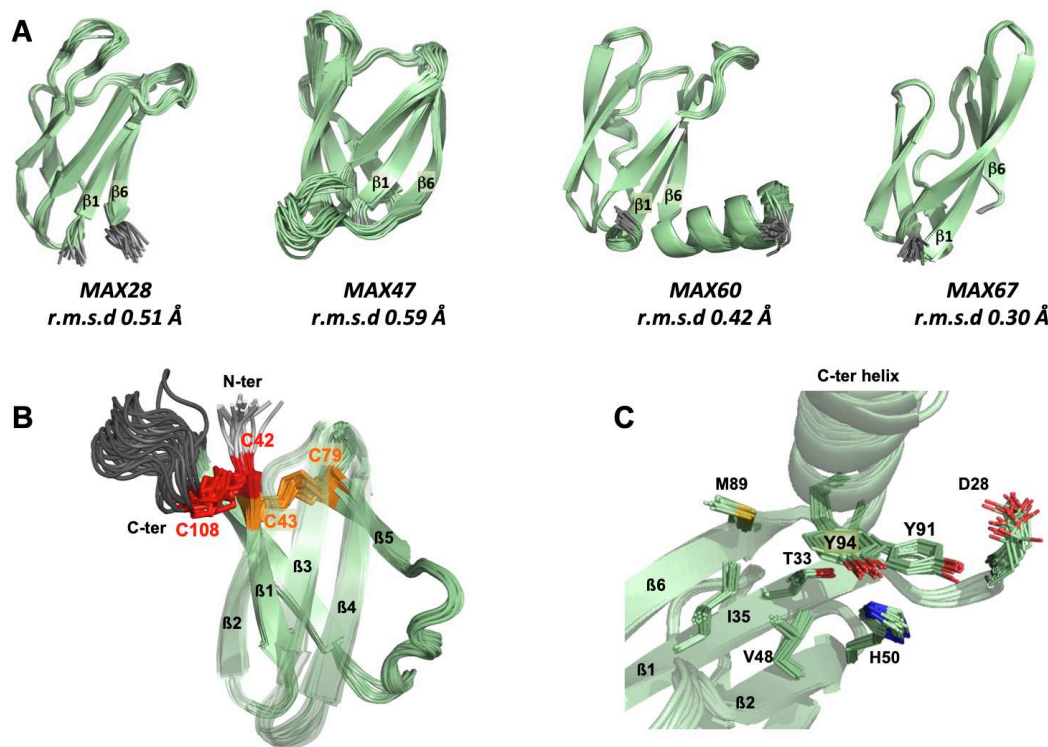


Fig 2. NMR structures of four MAX effectors. (A) NMR structures of MAX28, MAX47, MAX60 and MAX67 showing the superimposition and the r.m.s.d. of their 20 best conformers. The N- and C-terminal unstructured extensions before β1 and after β6, respectively, are not shown. (B) View of the two disulfides bonds, C42-C108 (red) and C43-C79 (orange) for NMR structure of MAX47. The loop between the end of β6 and the C-terminus is colored in dark grey. The β2, β3 and β4 strands are transparent. (C) Local environment of the two residues Y91 and Y94 in the C-terminal helix of MAX60.

Among the four MAX effectors, three proteins (MAX28, MAX47 and MAX67) displayed the characteristic MAX β -sandwich fold consisting of two triple-stranded β -sheets stapled against each other through a conserved disulfide bridge linking β 1 and the β 4- β 5 loop (Fig. 1). The two cysteine residues forming this salt bridge are the only residues that are highly conserved in MAX effectors. In MAX67, the β 1 and β 2 strands are longer than (10 a.a.) than their counterparts previously observed in other MAX structures. A slight divergence from the canonical MAX fold was observed for MAX60: the β 5 strand is replaced by a helical turn that prevents the formation of a regular β -sheet with β 4. In addition to the central MAX core, MAX28, MAX47 and MAX60 presented remarkable N- and C-terminal extensions. For MAX47, the 23 residue-long N-terminal sequence extending before the β 1 strand was enriched in serine residues and was not resolved in the NMR structure. The β 1 strand starts with two consecutive cysteine residues. The first cysteine makes a disulfide bond with the last C-terminal cysteine residue (C42-C108). The second cysteine in β 1 forms a disulfide bond with the cysteine in the β 4- β 5 loop (C43-C79) as expected in canonical MAX effectors. Both disulfide bonds are well defined in the NMR structure (Fig 2B). MAX60 has a C-terminal extension, which forms a well-defined α -helix. This C-terminal helix is attached to the structural core by hydrophobic contacts with the rings of two tyrosine residues (Y91 and Y94). In the NMR experiments, close contacts deduced from Nuclear Overhauser Effects (NOEs) data were found between residues D28 to T33 and H50 for tyrosine Y91, and residues T33, I35, V48 and M89 for tyrosine Y94 (Fig 2C). In case of MAX28, cleavage of the His-tag after affinity chromatography resulted in the precipitation of the protein that could not be purified with sufficient quality for structural studies. Nonetheless, the N-terminal His-tagged version was amenable to NMR analysis (Material and Methods). The 42

residue long C-terminal extension of MAX28 contains lysine-repeated motifs (KxxxK) and was predicted to be unstructured. The corresponding resonances were not assigned in the NMR spectra.

The four new NMR structures of MAX effectors were superimposed using TM-align with the corresponding TM-pred models that we previously generated by template homology modeling (Fig 3A). The quality of the models can be evaluated by the root-mean-square deviation (r.m.s.d) calculated between the observed and predicted structures and the TM-scores given by TM-align (a value of 1 meaning a perfect match). Comparison of the superimposed backbones shows that the overall MAX fold as well as the relative orientation of the two β -sheets forming the central β -sandwich were all well predicted, especially in the case of MAX28 for which the TM-pred model of the MAX domain matches very well the experimental structure (r.m.s.d.=2.11 Å), even for the loops joining the β -strands. MAX28 was also the effector with the highest estimated TM-pred score (0.75), in remarkably good agreement with the true TM-score (0.74) of the TM-pred model aligned to the NMR structure. Structural predictions of the MAX core were also very good for MAX67, except for the long strands β 1 and β 2 observed in the NMR structure that could not be accurately modeled, explaining the rather low TM-pred value proposed for TM-pred_MAX67. Some β -strands were also poorly defined in case of MAX47 and MAX60 whose models, compared to the NMR structures, exhibit also strong divergence for the connecting loop regions. For MAX47, the low reliability of the TM-pred model was anticipated by the TM-pred score (0.63).

AlphaFold2 reliably predicts MAX effectors core and extensions.

The recent release of Artificial Intelligence (AI)-based methods have demonstrated the high accuracy with which deep-learning software such as AlphaFold2 (AF2) can predict the 3D structure of most *structured* proteins [16]. We therefore decided to test the accuracy of AF2 to predict MAX effector structures by submitting the amino acid sequences corresponding to MAX28, MAX47, MAX60 and MAX67 for which the coordinates of the NMR structures we determined had not yet been released in the PDB. We used three different implementations of AF2 to generate the multiple sequence alignment (MSA) from which protein 3D models are predicted. The MMseqs2 and Jackhmmer implementations use MSAs generated automatically online or locally and that can include PDB templates, whereas the *Custom* MSA implementation uses MSAs provided by the user and was parameterized to not use PDB templates (see Materials and Methods). For each sequence query, the three MSAs were independently submitted to AF2 and the predictive quality of the top-ranked models was assessed thanks to the predicted local distance difference test (pLDDT) [16,17]. The pLDDT score scaling from 0 to 100 is a residue-level accuracy score computed by AF2 that provides an estimate of the confidence of each residue's predicted position in the protein structure. We considered the average pLDDT score for the overall protein, or only for residues within the predicted MAX core domain, herein called the MAX pLDDT score. The MAX pLDDT score allows better filtering of the AF-generated models, since it provides a quantitative measure of prediction quality focusing on the MAX core domain. For each MAX effector, the AF model having the highest MAX pLDDT score was selected and referred as its AF_MAX model (Fig 3).

291 The MAX core domain was very well predicted in AF_MAX47, AF_MAX60 and
 292 AF_MAX67 according to their high MAX pLDDT scores, close to or exceeding 90 (Fig
 293 3B and S5 Table). All the three selected models were obtained from the Jackhmmer
 294 AF2 implementation. Lower confidence score (74.1) was retrieved for the best AF2
 295 model of MAX28, generated using the *Custom* MSA implementation. Nevertheless,
 296 AF_MAX28 was very close to MAX28 experimental structure according to the
 297 average r.m.s.d. value (1.42 Å) calculated when superimposing the MAX core
 298 backbone atoms of the NMR conformers. Indeed, for all four MAX effectors, the MAX
 299 domain of the selected AF model displayed side-chain rotamers very similar to those
 300 observed in the experimental structures within the uncertainty of the NMR approach,
 301 i.e. density of NMR-derived constraints (Fig 3B).

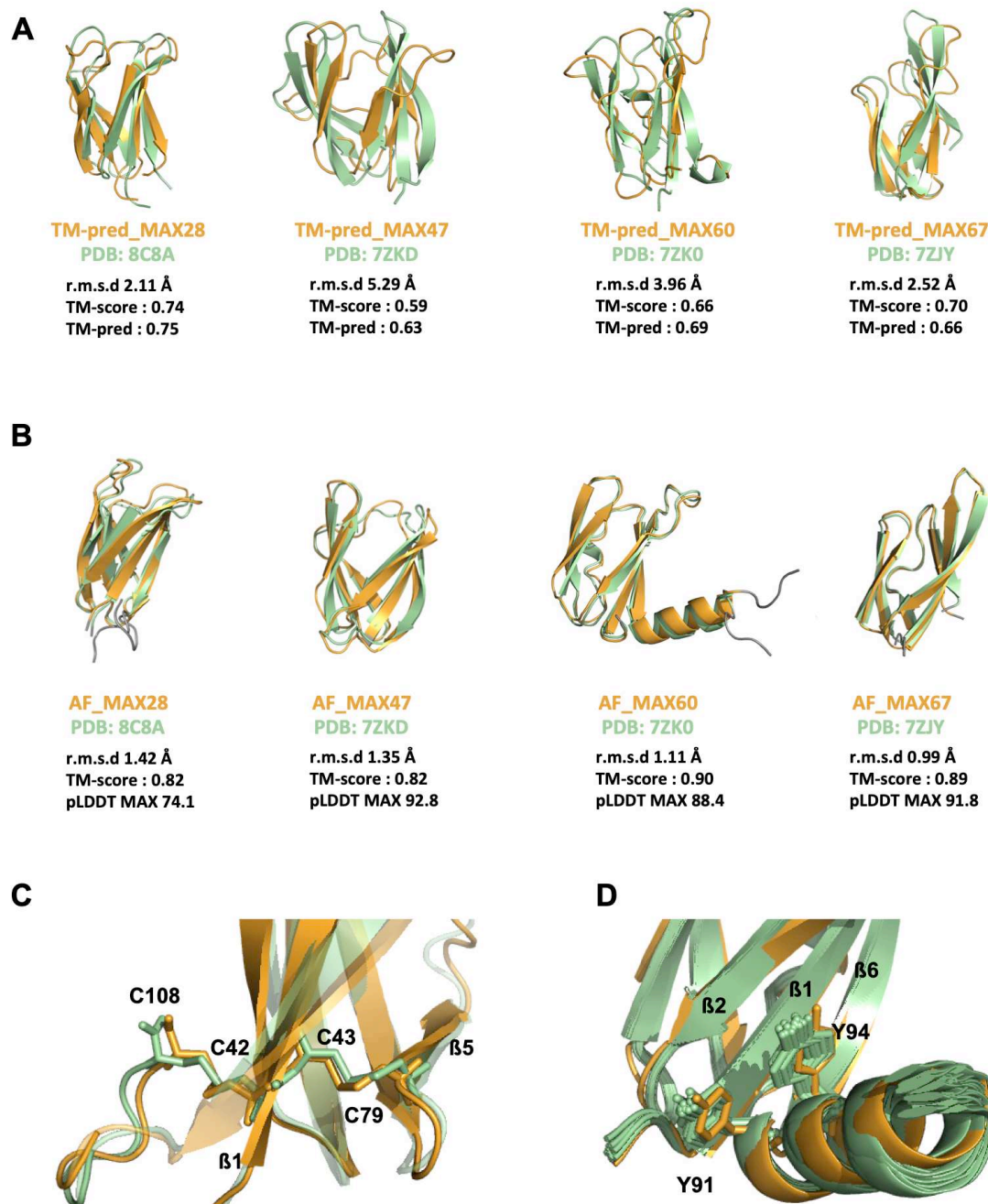


Fig 3. Comparison of newly determined NMR structures of MAX effectors with their TM-pred or AF predicted models. Superimposition of the four MAX effectors determined in this study by NMR shown by the best model (in green) and of their corresponding 3D models (in orange) predicted by hybrid multiple template modeling (TM-pred models shown in A) or AlphaFold2 (AF models shown in B). Metrics used for the quantitative assessment of the similarities between the predicted 3D models and their respective experimental structures are indicated: the root mean square deviation (r.m.s.d; the lowest, the best), the template modeling score (TM-score from TM-align, a value of 1

corresponding to a perfect match), *TM*-pred score (a predictive estimate of the *TM*-score). The N- and C-terminal boundaries were set according to the *TM*-pred models and did not include extensions determined in the NMR structures. (B) The *r.m.s.d.* between backbone heavy atoms of the superimposed NMR structure and AF models is given for the MAX domain only (Table S5), as well as the predicted local distance difference test (pLDDT) that was used to estimate the reliability of the AF predictions in the MAX core (MAX pLDDT score, Table S5). (C) View of the two disulfides bonds of MAX47, C42-C108 and C43-C79, as observed in the best NMR conformer and in the predicted AF_MAX47 model. (D) Local environment of the two tyrosyl side-chains of Y91 and Y94 in the C-terminal helix of MAX60 in the 20 NMR conformers and in AF_MAX60.

AlphaFold2 modeling also succeeded in predicting details within the core domains. The cysteine residue side-chains forming the conserved disulfide bond “1” are well defined in all four MAX effector models, as well as those forming an additional SS bond bridging the N- and C-terminal extensions in the experimental structure of MAX47 (Fig 3C). Another example of consistency between experimental structures and AF models was the remarkably well-defined position and orientation of the C-terminal helix of MAX60, in particular for two tyrosine residues whose aromatic side chains stack over the β 1- β 2- β 6 β -sheet of the MAX core (Fig 3D). For MAX28, both AF model and NMR structure were consistent in predicting unstructured N- and C-terminal extensions. Moderate deviations from the experimental structure were observed for residues in the C-terminus of MAX67 (S2 Fig).

Family portrait of AlphaFold2 MAX models

Given the high predictive quality of the AF-generated models of MAX effectors, we applied the same AF modeling strategy to all other *P. oryzae* OG representative members. The models were visualized to check the presence of the characteristic MAX core by inspecting the β -strand topology and formation of the conserved SS “1” disulfide bond (Pymol. v.1.6; Delano 2002). OG proteins showing significant

topological deviations from this canonical MAX fold were discarded. The strict presence of the short $\beta 5$ strand was not used as a filtering criterion. Among the 80 AF models that matched the canonical MAX structure (Fig 4), 57 had MAX pLDDT scores greater than 80 and 20 had MAX pLDDT scores ranging from 60 to 80. Only three OG proteins, OG26, OG73 and OG94, exhibiting a central core compatible with a MAX fold had a MAX pLDDT score below 60 and were not kept in our final selection of 77 validated MAX structures.

Among the 14 OG proteins that are not predicted to fold with the MAX topology, three (OG22, OG77 and OG85) were previously rejected based on their low TM-pred score and five (OG04, OG59, OG65, OG68 and OG81) had a TM-pred score under 0.6 (S1 Fig). Other OG proteins such as OG51 and OG54 that exhibited a TM-pred score above 0.6 compatible with a MAX structure displayed significant distortions from the canonical MAX fold when modeled by AlphaFold2.

For OG51, two models computed with MMseqs2 and the AF Jackhmmer implementation gave very similar models (backbone r.m.s.d. of 1.77Å) with pLDDT overall scores of 52.6 and 61.9, respectively. However, the C-terminal β -strand of OG51 had a parallel orientation relative to the first $\beta 1$ strand that was not compatible with the MAX topology. The best OG54 model had a pLDDT score of 59.4 but deviated from the MAX topology by the absence of the C-terminal $\beta 6$ strand, which was not accurately modeled.

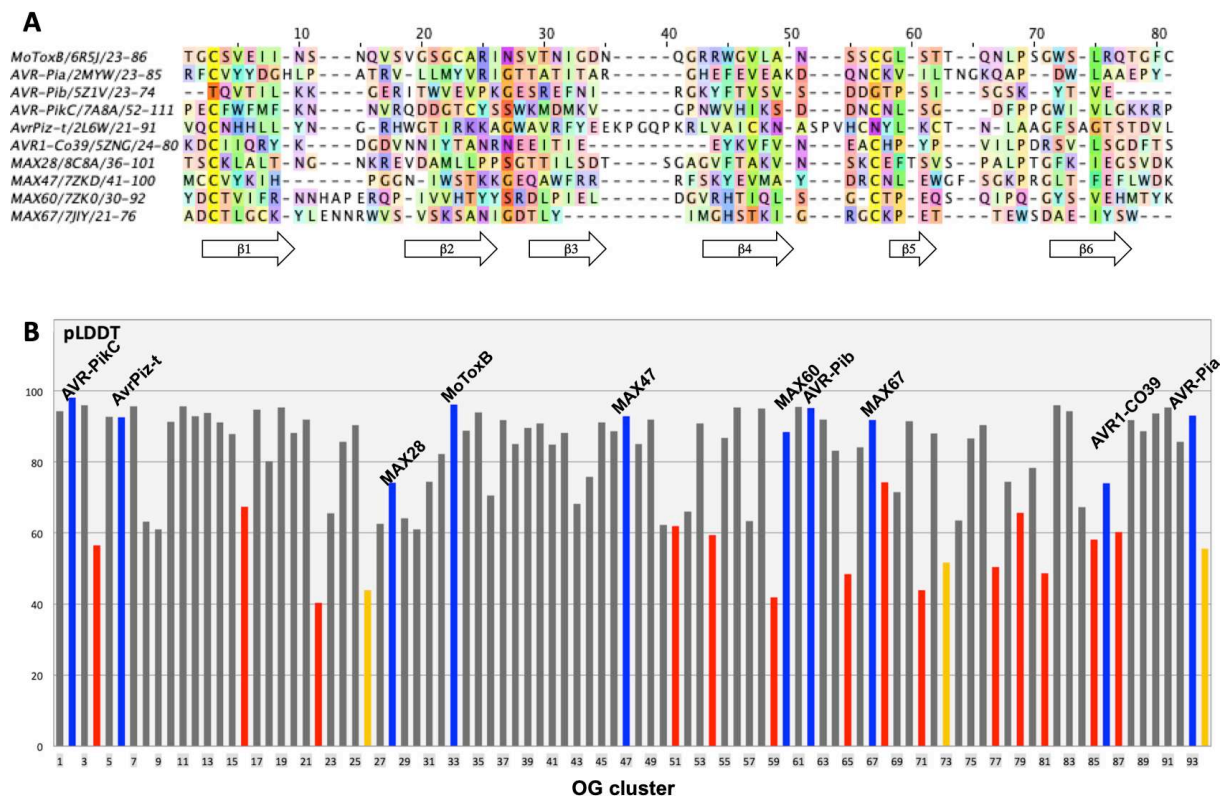


Fig 4. pLDDT scores of AF models for known and predicted MAX effectors.

(A) Structural alignments of experimentally determined MAX effector structures using MoToxB structure for reference. Residues are colored according to the Taylor scheme [18](Taylor, 1997) and conservation (above 15% threshold) is used as a shading factor.

(B) pLDDT scores of the best AF models selected for the 94 OG clusters of predicted MAX effectors with experimentally determined structures in blue, and OG clusters that displayed canonical MAX folds in grey. For these OG clusters we report the best MAX pLDDT score. OG clusters represented in red are the ones for which none of the models matched the canonical MAX fold, and in such cases we report the best overall pLDDT score of the model. MAX pLDDT scores of models that have a canonical MAX fold but a score below 60 are shown in orange. Full data is available in S5 Table.

The 14 OG clusters that gave inconclusive AF models were submitted to two other protein structure prediction web-servers, RaptorX [19] and RosettaFold [20]. None of the computed models displayed the canonical MAX fold, confirming that these OG cluster sequences were difficult to model and quite probably do not exhibit the expected MAX topology.

Variations around the canonical MAX fold

A statistical overview of the general structural features characterizing the 77 AF models of validated MAX effectors is given in Tables S7a and S7b. A unique member of the MAX family is MAX52, whose AF model consists of two MAX core modules in tandem. The MAX52 model was cut into two chains (MAX52A and MAX52B), each corresponding to a MAX core domain. In Fig 5A is indicated the average size of the β strands and connecting loops forming the conserved 6 stranded β sandwich that defines the canonical MAX fold, well represented by the MoToxB (MAX33) structure. β 1 and β 2 are usually of similar size and associate together with β 6 to form the longest anti-parallel β sheet, while β 3 and β 4 strands are usually shorter. Substantial variations around this common fold can be observed, notably in the C-terminal part of the MAX core where the short β 5 strand can be totally absent (MAX78 and MAX83) or replaced by a helix (MAX20), whereas the β 5 strand can range from 2 to 8 residues following a loop that can have up to 25 residues (MAX29) or present a short helix (MAX15, MAX60). The number of disulfide bonds stabilizing the protein can also greatly varied (Table S7a), from none in MAX61 and MAX62 (AVR-Pib) to three in MAX46 or four in MAX52. Besides of the conserved disulfide bond (SS “1”), which is a hallmark of the MAX domain, three types of additional disulfide bonds (SS “2”, “3” and “4”) are found in the observed or AF predicted MAX structures (Figs 5A and B). SS “4”, joining the N-terminus of β 1 to a C-terminal cysteine, is well defined in both MAX47 and MAX92, although it was not present in any of the previously determined MAX 3D structures that could serve as template. This disulfide bond was experimentally validated by our NMR structure of MAX47.

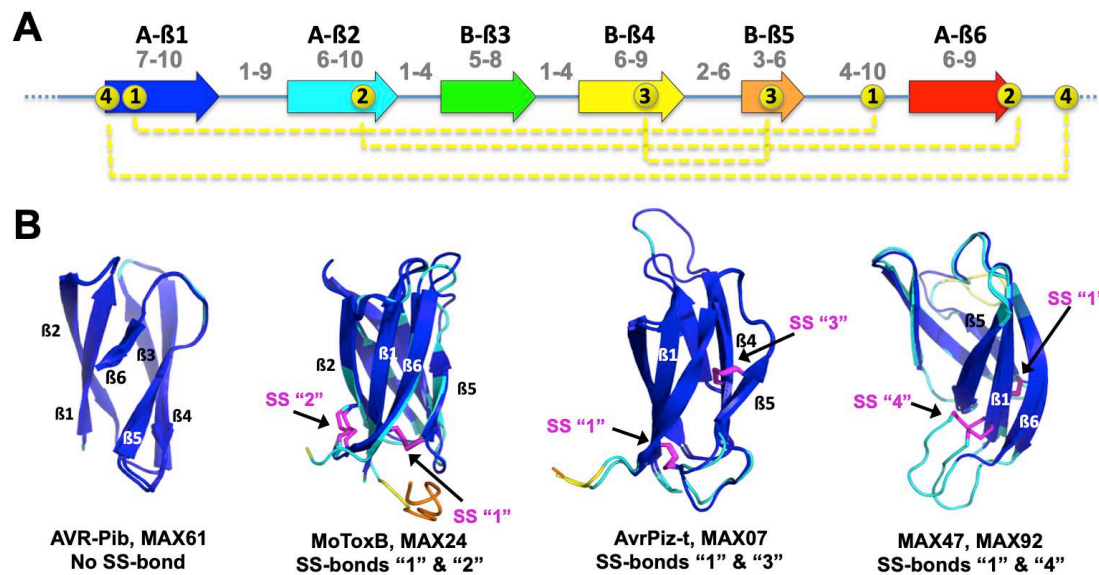


Fig 5. MAX domain structural features. (A) Average size range (indicated in grey) of β strands (arrows) and connecting loops forming the central β sandwich of the canonical MAX core, and of the N-ter and C-ter extensions. Average ranges are calculated in Table S7b. The 4 different types of disulfide bonds observed in MAX structures and models are indicated by dotted yellow lines. (B) Four different sets of structural models illustrating the variability of disulfide bond patterns. The AF models are colored according to their pLDDT score, by blue for high accuracy (>90), cyan for backbone at good accuracy (> 70), yellow for low confidence (> 50 and < 70) and orange for disordered (< 50). The disulfide bonds are shown in magenta, except for the AVR-Pib structure, which does not have a disulfide bond.

N- and C-terminal extensions

Over two-third of the 77 AF_MAX models possess peptide segments with 15 or more residues extending at one or both ends of the central MAX domain (Table S7a and S7b). Diverse length of these extensions, especially in C-terminal, can be observed among OG sequences belonging to the same OG cluster (e.g. OG01, OG02 or OG15 clusters in Table S1a). C-terminal extensions are also more numerous and usually longer than N-terminal extensions. They are often modeled by AF2 with well-defined secondary structures, such as additional β strands extending the β 2 β 1 β 6 sheet by one or two strands (e.g. MAX08, MAX12, MAX25), or a terminal

helix as observed in the model and solution structure of MAX60. There are also many examples where terminal extensions appear as unstructured regions that could not be modeled with high confidence by AlphaFold2. Long intrinsic disordered regions (IDRs) of more than 30 a.a. [21–23] may have diverse function in bacterial [24,25] and fungal effectors [26,27] and we had therefore searched for IDR signatures in MAX effector sequences using ESpritz prediction software [28]. Long IDRs were predicted for only a few MAX effectors and their presence was cross-validated for six AF_MAX models: in MAX15 (118 a.a.), MAX27 (36 a.a.) and MAX43 (43 a.a.) as N-ter extensions, and in MAX28 (42 a.a.), MAX53 (49 a.a.) and MAX78 (43 a.a.) as C-ter extensions. It thus appears that long IDRs is not a frequent feature among *P. oryzae* MAX effectors, present in less than 8% of all modeled structures. The NMR solution structure of MAX28 validated the unstructured nature of its C-terminal extension.

Structural classification of MAX effectors

Structural similarities between proteins can help to elucidate the function of an uncharacterized protein and infer its molecular evolution. Here we performed hierarchical clustering of the selected 77 MAX effector models with two protein structure alignment software, Dali [29] and TM-align [15,30] which use different criteria for similarity scoring of superimposed structures. The Dali Z-score relies on secondary structure pairing and is a good estimate of topological conservation while the TM-score is computed for the whole alignment and weights paired residues with low r.m.s.d. more strongly than those that are more distant. When analyzed independently, the structural alignment trees retrieved from these two clustering approaches did not reveal clear sub-families of MAX structures, as shown by the lack

of long internal branches in Fig 6. To facilitate the comparison of the trees, we differently colored the lines connecting each MAX model in both trees (see Materials and Methods).

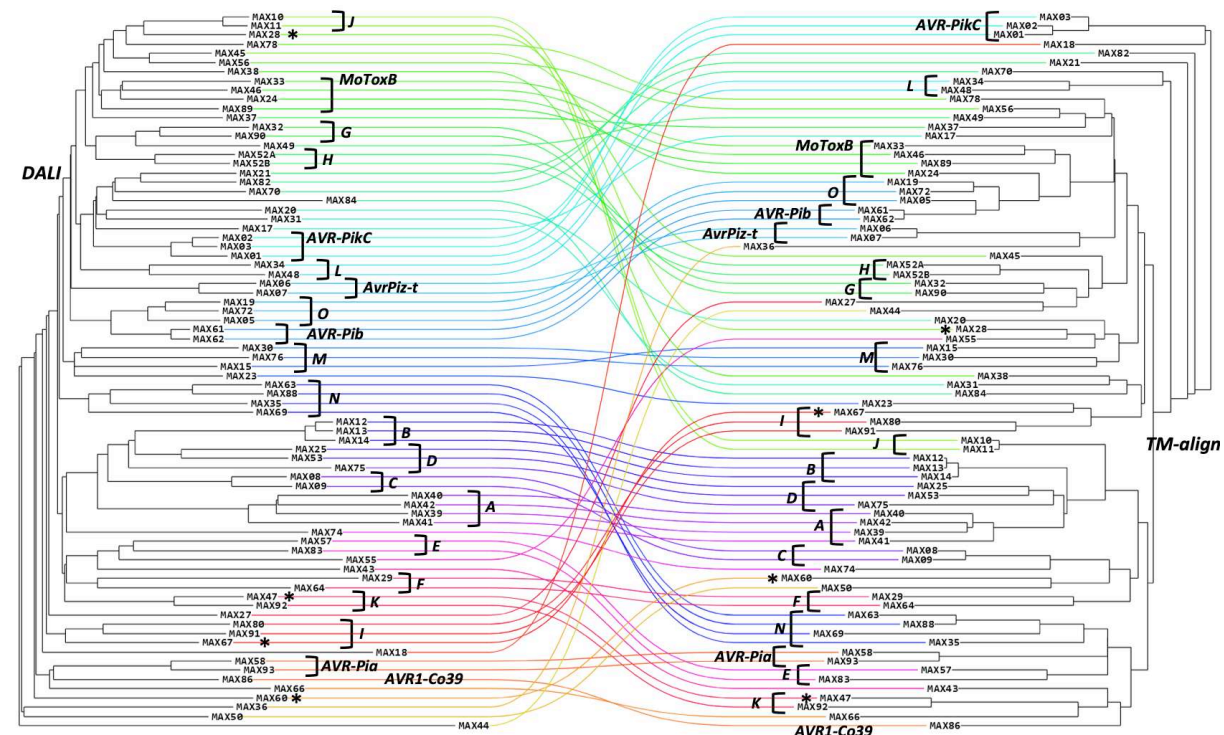



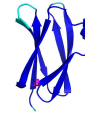

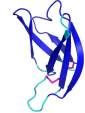

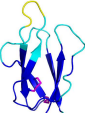
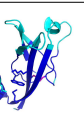




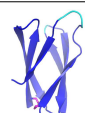
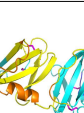







Fig 6. Comparison of the structural similarity trees of MAX effectors based on the Dali Z-score (left) and TM-align TM-score (right) of their superimposed AF models. Unstructured N- and C-terminal regions were removed from the AF_MAX models prior to the analysis. A line of a specific color connects each AF_MAX model in the Dali and TM-align trees. The MAX effectors with an experimental 3D structure are indicated by their name, or a star for the four novel MAX structures. The structural groups to which the MAX effectors were assigned are indicated by brackets and illustrated in Table 1 and S3 Fig.

In this representation, any bundle of lines of similar colors highlights a possible structural similarity between the models that was common to both clustering methods and that could define a group of MAX models. Each group of at least two models was visually inspected for additional secondary structures that could add to the MAX

core, the disulfide bond pattern as well as for specific structural features that fall outside the statistical average values reported in Fig 5A. Using this dual clustering method, we defined 15 groups of MAX models sharing common structural features, in addition to the 5 groups of well-established MAX effectors (AVR-Pia, AVR-Pib, AVR-PikC, AvrPiz-t and MoToxB). Groups A to G gather MAX models exhibiting major structured elements adding to the canonical MAX core: groups A and B contain models with 2 extra strands, groups C and D contain models with 1 extra strand, and groups E to G contain models with C-terminal helical extensions after $\beta 6$. Group H consists of the MAX52 tandem domains connected by a structured linker. In contrast, groups I to O correspond to plain MAX structures, without ostentatious decoration but presenting variations of the MAX fold specific to each group. The characteristics of this total of 20 MAX structural groups are summarized in Table 1 and illustrated with more details in S3 Fig. Only 6 groups exhibit a disulfide bond pattern with a specific SS bond adding to the conserved SS"1", and only the AVR-Pib group has no SS bond. The MAX models listed in Table 1 represent about two-third of the 77 MAX effectors that we validated in the present analysis. Several of them had been identified in a previous computational structural genomics study of *M. oryzae* strain 70-15 (see below) and are also listed in Table 1.

486 **Table 1. Structural groups identified in *P. oryzae* MAX effector family**

| Group | representative structure | MAX Id | SS(*) | Structural Specificities and Extensions | Group | representative structure | MAX Id | SS(*) | Structural Specificities and Extensions |
|----------|---|--|-------|---|----------|---|--|-------|---|
| A |  | MAX39, MAX40, MAX41, MAX42, MGG_16939T0, MGG_18062T0 | 1 | additional β 7 β 8 strands flanking one side of the β 2 β 1 β 6 sheet and C-terminal extensions after β 8 that are in helical conformations | I |  | MAX67, MAX80, MAX91, MGG_16175T0 | 1 | long β 1 strand paired with long β 2 or β 6 strands |
| B |  | MAX12, MAX13, MAX14, MGG_16619T0 | 1 | additional β 7 β 8 strands flanking one side of the β 2 β 1 β 6 sheet | J |  | MAX10, MAX11 | 1 | presence of a short helix in the connecting loop between β 5 and β 6 |
| C |  | MAX08, MAX09 | 1 | presence of the β 7 additional strand running antiparallel to the β 6 | K |  | MAX47, MAX92 | 1, 4 | disulfide bond "4" joining the N-terminus of β 1 and the C-terminal extension |
| D |  | MAX25, MAX53, MAX75, MGG_02635T0, MGG_15207T0, MGG_11304T0 | 1 | presence of the β 7 additional strand running antiparallel to the β 6 | L |  | MAX34, MAX48, MGG_15625T0, MGG_08992T0 | 1, 3 | malformed β 2 strand and anti-parallel β 4 β 5 strands stabilized by a disulfide bond |
| E |  | MAX57, MAX83 | 1 | long β 1 and β 6 strands, C-terminal helical extensions that are stabilized by hydrophobic interactions | M |  | MAX15, MAX30, MAX76, MGG_10282T0 | 1 | longer β 1 and β 2 strands and their connecting loops |
| F |  | MAX29, MAX64, MGG_17255T0 | 1 | C-terminal helical extensions that are stabilized by local residue-specific interactions (disulfide bond or hydrophobic residues) | N |  | MAX63, MAX88, MAX35, MAX69, MGG_02207T0 | 1 | unusually long loop making the connection between strands β 2 and β 3 |
| G |  | MAX32, MAX90, MGG_08469T0 | 1, 3 | long loop joining the β 1 and β 2 strands and helical C-terminal extensions that are not strictly conserved in their lengths and orientations | O |  | MAX05, MAX19, MAX72, MGG_12426T0, MGG_14793T0, MGG_18060T0 | 1 | Structurally similar to AVR-Pib. |
| H |  | MAX52 | 1, 3 | two MAX domains | AVR-Pib |  | MAX61, MAX62 | | Structurally similar to group O models. |
| AVR-Pia |  | MAX58, MAX93 | 1 | β 2 strand interaction with HMA (**) | AvrPiz-t |  | MAX06, MAX07, MGG_18041T0 | 1, 3 | very similar structures with the main difference for the β 3 β 4 connecting loop |
| AVR-PikC |  | MAX01, MAX02, MAX03, MGG_15972T0 | 1 | β 3 strand and N-terminal extension interacting with HMA (**) | MoToxB |  | MAX24, MAX33, MAX46, MAX89, MGG_17132T0 | 1, 2 | Structurally similar to ToxB with disulfide bond "2" |

487 The AF models are colored by their pLDDT scores (see legend of Fig 5). The groups with
488 major structural variations (addition of secondary structures) are listed in the left-hand
489 panels, including the MAX domain duplication of MAX52. The remaining groups, from I to O
490 that do not have additional secondary structures but displayed specific structural variations of
491 the MAX core domain itself are shown in the right-hand panels. To complete the overview,
492 the five groups of well-established MAX effectors (AVR-Pia, AVR-Pib, AVR-PikC, AvrPiz-t

and MoToxB) are shown at the bottom and highlighted in grey color. The MAX Id column gives the AF model identifiers of the MAX effector list reported in the present study (representative MAX model indicated in bold) and the corresponding MAX effectors reported by Seong & Krasileva, 2021 [3]; Seong and Krasileva, 2023 [4]; Yan and Talbot, 2023 [5] in the *M. oryzae* strain 70-15 are referred to by their MGG identifier (S8 Table).

(*) Type of disulfide bond as defined in Fig 5

(**) from crystallographic structures of complexes

Many MAX effectors are singletons

Singletons of MAX effectors are defined as those with no obvious structural relationship to other MAX effectors. They constitute a third (26/77) of the MAX effectors we modeled. In the majority of cases (17), these MAX effectors consist of a simple MAX core with unstructured N- and/or C-terminal extension(s). Among them is AVR1-CO39 (MAX86), which is specifically absent from the *Oryza*-infecting lineage, and whose structure has been experimentally determined. The remaining 9 singletons MAX effectors possess very diverse structured extensions besides the folded MAX core domain as illustrated in S4 Fig. Among these MAX effectors, MAX49 was already reported in *M. oryzae* strain 70-15 corresponding to MGG_08482T0 [5]. In MAX49, N-terminal and the C-terminal helices form a helix bundle structure, not observed in other MAX effector models. MAX74 has an additional β 7 strand running anti-parallel to β 6, as observed for group D models. Three other models have a β 7 strand, i.e. MAX36, MAX43 and MAX66, the latter having long β 1 and β 6 strands. Additional C-terminal helices were modeled with good accuracy in MAX55 and MAX60, but not in MAX44 and MAX84.

MAX domains exhibit very variegated surface properties

Comparison of the molecular surfaces of homologous proteins can highlight

common or specific features related to their function. This can be challenging in case of proteins that differ in size or have structural elements adding to their common fold. Here we have performed a detailed comparative analysis of the surface properties of the standalone MAX domains extracted from 49 AF_MAX models in which no structured regions are predicted to interact with the central core (S7a Table). For this subset of MAX domains, we computed SURFMAP [31] 2D projections of their molecular envelop and compare the distribution of different surface features i.e. exposed secondary structures, electrostatic potential, stickiness (Fig 7) and amino-acid polymorphism within the OG cluster to which belongs each representative MAX model.

The β 1-exposed surface is mostly discontinuous around the β 2 surface that is located at the *northern* pole of the projection (Fig 7C). The continuous β 3 surface lies below the β 2 surface and the discontinuous β 4 surface is found at the bottom of the projection. The β 6 surfaces are found to the *west* and *east* of the β 1- β 2 surface areas whereas β 5 surfaces are found on the most *eastern* areas. The electrostatic potential maps (Fig 7D and S2 files) reveal that MAX domain surfaces are more often positively charged than negatively charged or neutral, and that the molecular surfaces can appear entirely positive (e.g. MAX06 (AvrPiz-t), MAX23, MAX34, MAX47) or negative (e.g. MAX10, MAX38, MAX78, MAX86 (AVR1-Co39)), or present intense electrostatic patches (e.g. MAX02 (AVR-PikC), MAX58, MAX62 (AVR-Pib), MAX80). It is well known that positively charged regions in proteins are important for interaction with negatively charged macromolecules, such as nucleic acids and lipopolysaccharides [32], whereas negatively charged protein surfaces can be involved in membrane attachment or DNA mimicking functions [33–35]. In MAX47, we noticed that its unstructured N-terminal extension is rich in Asp residues,

suggesting that it could make transient interactions with the positively charged MAX core in the absence of its cellular target. In MAX62 (AVR-Pib), a surface loop region forms a strong positive patch (Fig 7C), which has been shown to be essential for the avirulence function of AVR-Pib and its nuclear localization in host cells [35]. Interestingly, a similar positive patch is visible on the surface of its structural homologs MAX61 belonging to the same structural group, as well as in MAX05 and MAX72 belonging to group O (Table1), suggesting that these effectors may also rely on this positive surface loop for their function. Similarly, AvrPiz-t displays a positively charged surface partially involving lysine residues that are required for AvrPiz-t avirulence and virulence functions in rice [14]. Inversely, while the surface of MAX86 (AVR1-CO39) is strongly negative, that of MAX93 (AVR-Pia) is neutral, yet both AVR1-CO39 and AVR-Pia interact similarly through their β 2 strand with the HMA domain from the rice immune receptors RGA5 [36] and Pikp-1 [37], respectively.

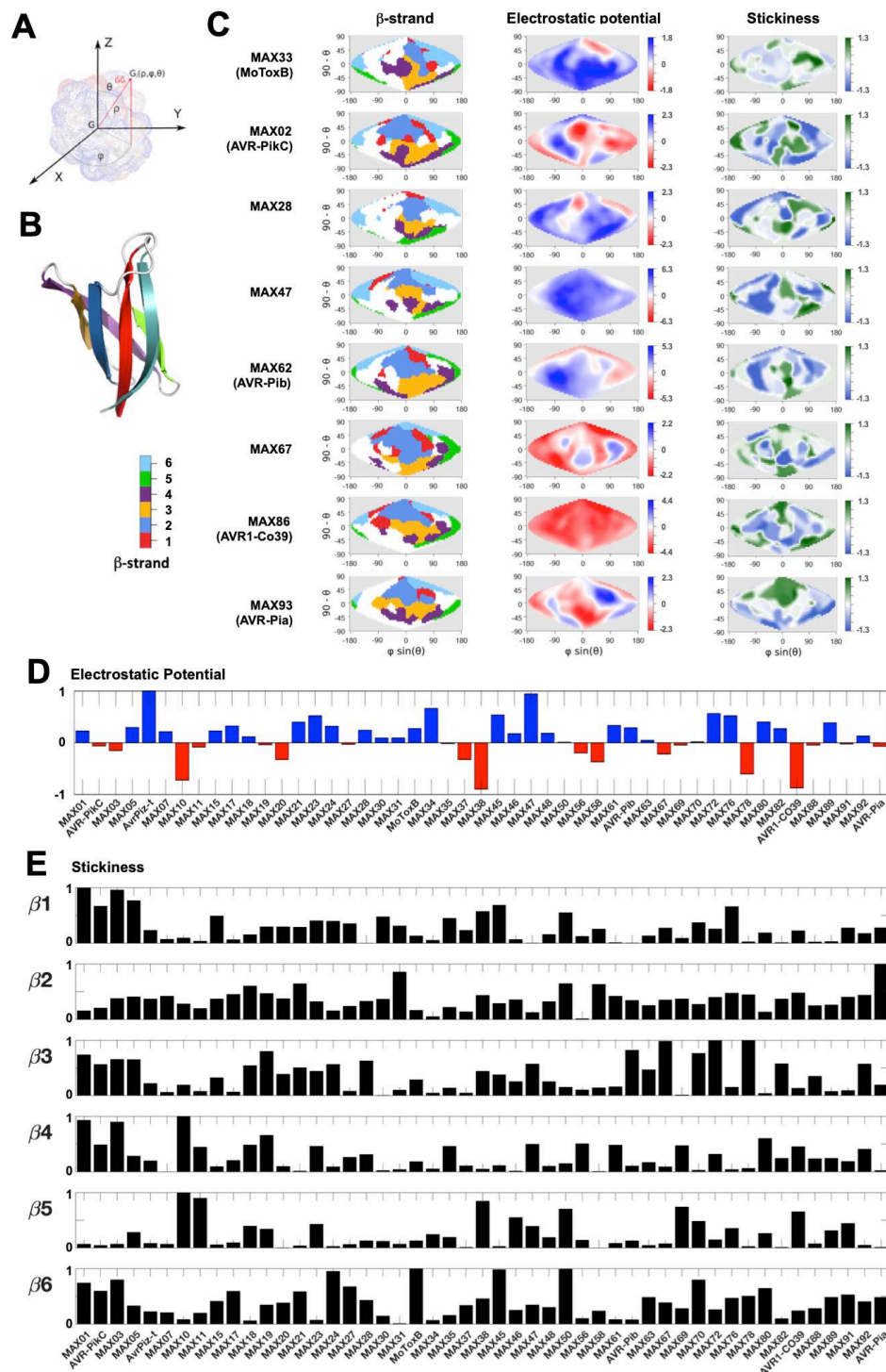


Fig 7. Surface properties of the MAX core domains.

Surface properties of MAX core domains computed and represented using SURFMAP. (A) Schematic of calculation of the spherical coordinates (from Schweke et al., 2022). The coordinates of each surface particle G_i is expressed in spherical coordinates (ρ, φ, θ) , where ρ represents the distance of the particle G_i to the center of mass G of the protein, φ is the angle between the X axis and the projected vector $\overrightarrow{GG_i}$ in the plan $(\overrightarrow{GX}, \overrightarrow{GY})$, while θ is the angle between the vector $\overrightarrow{GG_i}$ and the Z axis.

B) MoToxB structure showing the 6 β -strands of the MAX core with the color code used for the surface representation in panel C. **C)** 2D maps of exposed β -strands, electrostatic potential and stickiness of the molecular surfaces calculated by SURFMAP for MAX domains extracted from AF2 models of MAX effectors with known structure. N- and C-terminal extensions were discarded and the MAX core 3D models were all superimposed to AF_MAX33 (MoToxB) giving a reference frame for the Sanson-Flamsteed 2D projection computed surfaces. The β -strand maps use the color code given in panel B, the electrostatic potential maps are scaled in the indicated kT/e units and the stickiness (related to hydrophobicity) scale is that defined by Levy E. D., 2010 [38]. **D)** Comparison of overall surface electrostatic potentials of MAX core domains, summed over the entire molecular surface and normalized by the highest absolute value calculated for the subset of 49 MAX effector models (S2 files). **E)** Relative surface stickiness of MAX core β -strands. Stickiness values were summed for residues forming each of the 6 β -strands of the MAX core domains and normalized by the highest value calculated for each strand in the subset of 49 MAX core models.

Wide divergence is also observed in the surface stickiness of the MAX domains. Surface stickiness is mostly related to surface hydrophobicity and reflects the propensity of each amino acid to be involved in molecular interfaces [38]. For AVR-Pia, the HMA binding site correlates well with the presence of a large hydrophobic patch on the surface (Fig 7C and panel C in S5 Fig) and a very sticky β 2 strand, also present in MAX31 (Fig 7E). This is however not the case for AVR1-CO39 whose surface hydrophobicity is limited except in strand β 5. This strand is particularly variable in length and surface properties, exhibiting high stickiness in only a few MAX effectors (e.g. MAX10, MAX11 and MAX38) where it could contribute to the binding site of host target proteins. For the AVR-Pik group (MAX01, MAX02 and MAX03) surface stickiness is high in β 1 and sticky patches are also observed in strands β 3, β 4 and β 6. In all these effectors, the β 3 stickiness could serve in an interaction with strand β 4 of HMA domains, as observed in complexes of different MAX02 effectors with the HMA domain from Pikp-1 or from the rice protein OsHIP19 targeted by AVR-PikF [8–10]. Other MAX effectors (e.g. MAX67, MAX72 and MAX78) possess a highly sticky β 3 strand that could also associate with the β -strand of an HMA domain

or other type of protein domain. In the crystal structures of the AVR-Pik effectors, the anti-parallel β 1- β 6 strands of the MAX core are making hydrophobic contacts with residues in their N-terminal extension which adopts a conserved extended conformation and considerably expands the binding interface with the HMA (S5 Fig). In MAX structural groups A to D of Table 1 (not included in the present subset), a sticky β 6 strand often associates with an anti-parallel β 7 extending the MAX core β -sheet. Similarly, the highly hydrophobic β 6 strand present in MAX33 (MoToxB), MAX45 and MAX50 could interact with target proteins through an antiparallel β -strand arrangement.

Altogether, this analysis highlights the very variegated surface properties exhibited by the *P. oryzae* MAX effectors. In spite of sharing a common fold, these sequence diverse proteins retain very high diversity at the structural level. On the other hand, sequence conservation is high inside each OG cluster with average conservation scores in strands and loops close to the maximum conservation score of 9 (S7c Table). Three clusters display low conservation scores in β 2, β 3 and β 6 strands represented by MAX47, in β 2 and the loop joining β 4 to β 5 for MAX63, and in strands β 4 and β 5 for MAX70, and accordingly, higher polymorphism on their surfaces (S6 Fig and S2 Files).

Discussion

We initially used hybrid multiple template modeling that combines information from multiple template structures to predict the core of MAX effector structures. The best models were selected according to their predicted TM-score (TM-pred), a commonly used measure to assess the structural similarity between predicted models and the true native structure. By comparing new experimental MAX effector

NMR structures with their corresponding TM-pred models indicated the low accuracy of the models, pointing to the limits of template-based homology modeling [39] and the need of alternative modeling strategies to model MAX effectors.

Ab initio modeling

Recently, *ab initio* modeling, specifically using Rosetta and the two web servers Robetta and QUARK, was applied for predicting the structures of already known MAX effector proteins of *Magnaporthe oryzae* [40]. The Rosetta *ab initio* modeling approach generated models with the best overall TM-scores, with AVR-Pib achieving the highest TM-score. The exception to this trend was AVR-Pik, for which the QUARK method produced the best model with a TM-score of 0.89, compared to a TM-score of 0.51 in Rosetta. Overall, the study highlights the strengths and limitations of *ab initio* modeling for predicting the structures of fungal effector proteins. While *ab initio* methods can provide valuable insights into the overall fold and topology of proteins, accurately predicting detailed secondary structures remains challenging, especially in the cases where the TM-scores are relatively low. The performance of different *ab initio* methods can also vary depending on the specific protein being modeled. To address the issue of missing secondary structures or other structural defects, further refinement techniques or hybrid methods can be employed. These approaches aim to improve the accuracy of the predicted models by incorporating additional information, such as experimental data, molecular dynamics simulations [41], fragment assembly [42], or consensus modeling that can be used to refine and improve the quality of predicted models. Although this can improve the robustness and accuracy of the predicted models, it involves additional computational steps and requires the availability of multiple predictions.

Modeling of MAX effectors from *M. oryzae* strain 70-15 using deep learning

TrRosetta and AlphaFold are novel computational methods based on deep learning techniques to predict protein structures from amino acid sequences, bypassing some of the computationally-intensive steps required by traditional methods. The MAX family repertoire of *M. oryzae* strain 70-15 was investigated and models were generated by computational methods mostly using TrRosetta [3] and AlphaFold [4,5]. The first study (TrRosetta models) identified 11 MAX candidates and similar population sizes of 26 and 32 MAX candidates were reported for the two other AlphaFold studies, respectively. While 10 MAX of these candidate models were commonly identified and systematically assigned to MAX effectors by all three studies, another set of 22 MAX effectors were identified in less than three studies (S8 Table), indicating the difficulties in model selection based on pTM-score and in detecting structural similarity using methods like CATH [43] and SCOPE [44].

Most of the MAX effectors that were previously reported in the TrRosetta and AlphaFold studies were also identified in our analysis (Table 1 and S8 Table) with the exception of OG54 that we did not select as a MAX effector. MAX members of the groups C, E and H were not found in these previous reports while the equivalent sequences in the *M. oryzae* strain 70-15 for MAX members of groups J and K could not be found.

In our study we used the pLDDT score (predicted *Local Distance Difference Test*), which provides a residue-level assessment of the confidence or accuracy of each residue's predicted position in the protein structure. By focusing on the pLDDT scores within the MAX folded region, we specifically evaluated the local accuracy of the predicted structure within the MAX core domain. This localized scoring approach enables a more focused evaluation and filtering of the protein structure predictions,

and allows identification and selection of the best models with higher accuracy and reliability within the specific region of interest. By comparing the experimental results from NMR with the corresponding AF models, we were able to assess the accuracy and reliability of the AF predictions.

Venturia inaequalis MAX-like effectors

V. inaequalis is an ascomycete fungus, in the *Venturiaceae* family, responsible for apple scab disease. Assessing models of *V. inaequalis* MAX-like effectors [45] against the criteria we defined here to assign MAX effectors to subfamilies, revealed that none of the models fitted into any of the MAX subfamilies. Indeed, *V. inaequalis* MAX effectors present three remarkable disulfide bonds. One is the canonical “1” bond found in other MAX effectors, while the remaining two were not found in any of the MAX effectors from *P. oryzae*. Moreover, MAX-like effectors of *V. inaequalis* usually possess a C-terminal helical extension connected to the MAX core domain via a specific disulfide bond that was not observed in any MAX from *P. oryzae*. This makes these newly discovered MAX-like effectors from *V. inaequalis* another subfamily with unique sequence/structure features [45]. As *V. inaequalis* exclusively colonizes and releases effectors in the subcuticular host environment without penetrating the underlying epidermal cells, their function, and thus targets, are probably fundamentally different from the other studied MAX effectors from *P. oryzae*.

MAX effector AlphaFold models predicted in 120 *P. oryzae* genomes

Clustering of the 77 MAX effector models successfully predicted by AlphaFold allowed us to distinguish 15 subfamilies. Our study showed that, beyond the well-

known conserved MAX core, the MAX superfamily is characterized by an important structural diversity shown by additional structured regions in the C-terminal portions of several of its members. Specifically, these include additional strands observed in groups A to D and helical extensions observed in groups E to G. These regions may play a role in protein-protein interactions or contribute to the effector's overall functionality. On the other hand, long intrinsically disordered regions (IDRs) were rarely observed in only six MAX effectors. IDR regions lack a stable 3D structure and exhibit conformational flexibility, allowing them to interact with multiple binding partners and fulfill various functions [46] but are difficult to predict from the sequence [47].

Furthermore, the study also identified more modest structural variations within the MAX core for seven groups, labeled from I to O. These variations indicate that even within the core structural framework of the MAX effectors, there are subtle differences that distinguish these groups from each other. The classification given in Table 1 can be improved by incorporating surface properties. Thus, the AVR-Pib and O groups could be agglomerated, since they are structurally similar and members of the O group have electrostatic surfaces related to AVR-Pib.

Notably, our study uncovered a domain duplication event within one of the MAX effector clusters (group H). Other dual-domain effectors have been described in recent studies, i.e. the Fol dual-domain effectors (FOLD) [48] and effectors predicted from *Puccinia graminis* [4]. The discovery of dual-domain effectors, including the domain duplication found in one of the MAX effector cluster, adds to our understanding of the diversity and complexity of effector proteins. These dual-domain effectors likely have evolved to possess multiple functional domains that contribute to their virulence or interaction with host plants.

β1 and β6 surface stickiness of AVR-Pik effectors

The AVR-Pik AF models display high surface stickiness on β1 and β6 strands that could serve to anchor residues from the N-terminal extensions of these effectors to their MAX core domains. While there are multiple experimental structures of AVR-Pik in complex with HMA domains, whether the structure of the free AVR-Pik effector differs when not in complex with an HMA domain remains an open question. In the AF models of MAX01, MAX02 and MAX03, the first 10-residues at the N-terminus are unstructured. These are followed by a stretch of 20 residues, which are well defined according to their pLDDT scores but without regular secondary structure, and which adopt the conformation observed when the AVR-Pik effectors are in complex with an HMA domain. Alternative AF models computed with the *Custom* MSA implementation that does not use PDB templates showed different conformations for this stretch of 20 residues, from totally unstructured (MAX01) to helical tendency (MAX02). Based on these AF calculations we could expect that when free, AVR-Pik effectors have a N-terminal extension alternating between different conformations but we cannot exclude that this extension, while not having canonical secondary structures, could participate to the overall stability of the AVR-Pik effectors. Truncation mutants may serve to validate this hypothesis, however mutations within or truncations of *a priori* unfolded protein regions may have deleterious effects not only on the structure stability, as shown for N-terminal truncations of AVR-PikD (pages 87-88 in ref. [49]) but also and more specifically on the overall folding process of the protein. Recently, we used HP-NMR (high Hydrostatic Pressure NMR) [50,51] to study the folding/unfolding of AVR-Pia, AVR-Pib [52] and MAX60 [53]. In the case of MAX60, we observed an early folding intermediate involving β1, β6 and the C-terminal helix that is a specific extension of this MAX effector, and mutants lacking

this helix were not sufficiently stable to be purified. This demonstrates that the presence or absence of additional sequences outside the core can have profound impacts on the folding of these effectors.

Concluding Remarks

Beyond the scope of information derived from the primary sequence, structural information expands our understanding of biological processes at the atomic level. Moreover, the three-dimensional structures of the different partners can be indicative of the evolutionary pressure exerted on a biological system. This is far to be trivial especially in the case of sequence divergent effectors that are also found to form a significant structural family. The presented prediction pipeline, associated with modeling using AlphaFold already showed a successful prediction rate of MAX effectors of nearly 80%. The quality of these results has been proven by the experimental resolution of four new MAX effectors MAX28, MAX47, MAX60 and MAX67, which revealed the outstanding accuracy of the predictions when superimposed with their respective model, especially in the position and orientation of the side chains and secondary structures. A subset of 20% of the OG cluster sequences resulted in ambiguous models (unreliable or with major structural deviation of the expected MAX fold) pointing out the limits of *de novo* prediction on such divergent sequences. This emphasizes the significance of the experimental structural elucidation, which remains the key evidence even if known to be challenging and resource consuming. Nonetheless, structure modeling will provide solid foundations for the structure characterization or the study of interacting biological entities, when limited or no information at all is available. The surface stickiness mapping while not unambiguously informing of what could be the protein

interface on the MAX domain surface, which is in contact with the host target, may help to build hypothesis and to design plant biology experiments for validation. Linked to these predictive studies of interfaces between MAX effectors and their targets are new developments in AlphaFold2, such as improved prediction of protein-protein interactions [54] or screening of interactions between proteins [55].

The MAX family effector proteins provide an example where the core structural platform has the plasticity to adapt extensions constituting new potential interacting modules with target proteins. This structural variability within effector families is important for their functional diversity and adaptability. By adding extensions or new modules, effectors can acquire novel functionalities, interact with different host targets, or modulate different host immune responses.

Materials and Methods

Experimental Structures

MAX28 Protein expression and purification.

Protein expression and purification experimental details for MAX47, MAX60 and MAX67 are available in [56] Lahfa et al. 2022. For MAX28 we followed essentially the same protocol than for the other MAX effectors for producing the ^{15}N -labelled NMR sample but the His₆-tag was not cleaved to keep the protein soluble. Uniformly labeled ^{15}N MAX28 was expressed in E. coli BL21 (DE3) cells (Invitrogen, Thermo Fisher Scientific, Waltham, USA) from a homemade plasmid pDB-his-CCDB-3C (courtesy of Frederic Allemand, CBS Montpellier, France). Protein expression was carried out in $^{15}\text{NH}_4\text{Cl}$ (1 g/l) enriched M9 medium. Cells were grown at 37 °C until reaching an OD600 = 0.8 and then, expression proceeded overnight at 30 °C after induction by addition of 0.3 mM IPTG. Cells were harvested by centrifugation, re-suspended in denaturing buffer (50 mM Tris, 300 mM NaCl, 1 mM DTT (dithiothreitol), 8 M urea, pH 8) and lysed by ultra-sonication. The supernatant containing the unfolded protein was applied to a HisTrap HP 5 ml affinity column (Cytiva, Freiburg im Breisgau, Germany). The His₆-tagged protein was eluted in 50 mM Tris, 300 mM NaCl, 1 mM DTT, 8 M urea, pH 8 with an imidazole gradient up to 500 mM. At this step, MAX28 was directly dialyzed against 10 mM Na Phosphate, 2 mM DTT, 150 mM NaCl, pH 6.8 buffer in order to remove imidazole and urea, allowing the refolding of the protein. The MAX28 samples were then concentrated using Amicon Ultra Centrifugal Filter Devices (MW cutoff 3000 Da), (Merck Millipore, Burlington, USA) prior to size exclusion chromatography (SEC) using HiLoad 16/600 Superdex 75 pg column (Cytiva). Fractions containing protein were pooled, concentrated to 0.4 mM and stored at -20°C. All NMR experiments were carried out

at 27°C on a Bruker Avance III 800 MHz or Bruker Avance III 700 MHz spectrometer, both equipped with 5 mm z-gradient TCI cryoprobe. NMR samples consisted on approximately 0.4 mM ¹⁵N-labeled protein dissolved in 10 mM Na-Phosphate buffer (pH 6.8) and 150 mM NaCl with 5% D₂O for the lock.

NMR Structure determination of MAX28, MAX47, MAX60 and MAX67.

¹H chemical shifts were directly referenced to the methyl resonance of DSS, while ¹⁵N chemical shifts were referenced indirectly to the absolute ¹⁵N/¹H frequency ratio. All NMR spectra were processed with Topspin 3.6 (Bruker) and analyzed with Cindy 2.1 (Padilla, www.cbs.cnrs.fr). Assignments for MAX28, MAX47, MAX60 and MAX67 have been deposited to and are available from the BMRB data bank under the accession entry 34782, 34731, 34730 and 34729, respectively.

The NMR structures were determined from the NMR constraints listed in S4 Table that were obtained as follow. NOE cross-peaks identified on 3D [¹H, ¹⁵N] NOESY-HSQC (mixing time 150 ms) were assigned through automated NMR structure calculations with CYANA3 [57,58]. Hydrogen bond restraints were derived using standard criteria on the basis of the amide ¹H / ²H exchange experiments and NOE data. When identified, the hydrogen bond was enforced using the following restraints: ranges of 1.8–2.0 Å for d(N-H,O), and 2.7–3.0 Å for d(N,O). Dihedral restraints were obtained from TALOS-N [59] analysis of backbone atom chemical shifts for MAX47, MAX60 and MAX67. For the final list of restraints, distance values redundant with covalent geometry were eliminated and disulfide bonds that were consistent with short distances between cysteine residues were added.

A total of 200 three-dimensional structures were generated using the torsion angle dynamics protocol of CYANA3 from NOEs, hydrogen bonds and disulfide bond

restraints (S4 Table). The 20 best structures (based on the final target penalty function values) were minimized with CNS 1.2 according to the RECOORD procedure [60] and analyzed with PROCHECK [61]. The rmsds were calculated with MOLMOL [62]. All statistics are given in S4 Table.

The structure coordinates have been deposited at the Protein Data Bank under the following accession codes: MAX28 (PDB_8C8A), MAX47 (PDB_7ZKD), MAX60 (PDB_7ZK0), MAX67 (PDB_7ZJY),).

TM-pred MAX models Web Table

Homology models of each OG representative sequence relative to each 3D template were built using MODELLER v9.1 [63] with several alternative query-template threading alignments as described in [7]. The top-5 models were selected according to the TM-pred scoring function and are given in <https://pat.cbs.cnrs.fr/magmax/model/> Web page.

The Web table has the following columns: Group (OG cluster), Score (composite evaluation score of the best model -best scores are in red, worst are in blue-), Dfire, Goap, Qmean, E1D, E2D, E3D (individual evaluation scores of the best model), Alignment (aligned identifier sequences), Identifier (protein identifier of the orthologs prioritizing *Oryzae* infecting strains). Structural models and alignments are available by clicking on each OG cluster in the first column. A multiple sequence alignment of non-redundant orthologous proteins is displayed at the top of the page, starting with the modeled representative sequence. For each OG cluster given in [7] we further filtered out redundant sequences using CD-HIT [64] (S1 Table). The representative sequence of each OG cluster was determined to be the sequence sharing the highest sequence identity with a consensus sequence derived from the OG cluster

sequence alignment by MAFFT [65] (S2 Table). Signal peptide prediction before the cleaved residue (cs.SIGNALP41), mean hydrophobic index (ih.MEAN), sequence conservation (1D.CSRV), alternative alignments and model secondary structures (2d.STRIDE) are displayed below the sequence alignment. Sequence conservation scoring implemented in PAT [66] was calculated according to Sonnhammer and Hollich, 2005 [67] with a Gonnet matrix [68]. At the bottom of the page, the 5 best models can be displayed using different representations and color schemes. Models can also be downloaded in PDB format.

Modeling by AlphaFold.

For each OG representative sequence we computed three AF models differing by the way of building multiple sequence alignment (MSA). The MMseqs2 MSA was obtained from the MMseqs2 [69,70] web server as implemented in the ColabFold version of AlphaFold 2.0 [71]. We also used the version of AlphaFold 2.2.0 that builds MSAs by Jackhmmer on uniclust, mgnify and uniref90 databases. These two implementations use PDB templates. Finally, a *Custom* MSA was build from Muscle_v3.8.31 [72] by inserting (-profile option) the query sequence on top of a previously computed MSA, termed $\beta 1\beta 4_MSA$. The $\beta 1\beta 4_MSA$ was build from a Muscle alignment of the OG sequences (S1 Table) by filtering out those having the two flanking cysteine residues in the $\beta 1$ and in the loop between $\beta 4$ and $\beta 5$ strands not correctly aligned to the 8 3D template sequences. The $\beta 1\beta 4_MSA$ was further processed by truncating the sequences by eliminating residues (-2 included) before and (+2 included) after the first and last aligned cysteine residues, respectively, and filtering out for redundant sequences by CD-HIT, giving a total size of 247 aligned sequences (S6 Table). For each query, the consistency of the *Custom* MSA was

determined by checking the correct alignment of the cysteine residues in the query and in the appended $\beta 1\beta 4$ _MSA. When consistent the *Custom* MSA was converted to a3m format by the reformat.pl script [73] and directly used as input in the ColabFold implementation of AlphaFold 2.0 calculations that was setup without the use of PDB templates. *Custom* MSAs could not be built for OG61 and OG62 from absence of cysteine residues in their primary sequences and were not consistent for OG15, OG27, OG71, OG81, OG85 and OG92.

The quality of each model was assessed by the pLDDT overall score [74]. The correct MAX topology was verified by visual inspection (Pymol v.1.6 Delano 2002). For models having the MAX topology, a MAX pLDDT score that was an average score of residues in the MAX core domain (including residues from $\beta 1$ to $\beta 6$) was calculated. For each query, the best AF MAX model was selected when the MAX pLDDT score was above 60.

Dali implementation and search

A standalone implementation of DaliLite.v5 [75] was used for this work. For the all-to-all clustering by Dali we first discarded *unstructured* stretches in each model. For this, the *structured* domain of each model was defined by taking the STRIDE [76] output, and filtering for the first residue in the first and last residue in the last secondary structure (helix or strand), respectively (S7 Table). The model of MAX52 was split in two chains A and B each containing a MAX domain. All these *structured* domains were used for clustering with Dali Z-scores excluding *de-facto* unresolved protein regions without losing important structural information.

TM-align scoring and side-by-side plot with Dali Z-score tree.

The distance between each pair of AF models that were used for Dali clustering was estimated by the TM-score obtained from TM-align after pairwise model superposition. A classification tree was then inferred from these pairwise distances using FastME [77]. Finally, Fig 6 was obtained by joining identical models in the FastME tree and in the Dali tree, respectively, by a line of the same color.

Surface properties of MAX core domains.

A subset of 49 MAX effector AF models, each consisting of a MAX core domain and optional N- and/or C- *unstructured* extensions (S7 Table) was defined by discarding AF models having N- and/or C-terminal *structured* extensions (listed in the groups A to H in Table 1 and in S4 Fig). All MAX core domains of the 49 AF models were superimposed to the reference MoToxB structure with their β 1 strand vertically aligned to the Z Cartesian axe giving a reference frame for the Sanson-Flamsteed 2D projection computed using SURFMAP [31]. Their surface properties including stickiness and electrostatics (APBS) [78] were computed by SURFMAP and are given in S2 File. The temperature factor column of the PDB files was used to encode the color of the exposed surface of the six β -strands, from 1 to 6, respectively. The sum of the surface stickiness positive values of each individual β -strand was computed by filtering SURFMAP surface stickiness output and are reported in Fig 7D. The amino-acid conservation scores given for each OG cluster to which belongs each representative MAX model were used to color encode the surface from white for high conservation score of 9, light blue colors for intermediate conservation scores (from 8 to 6), sky-blue for low conservation score of 5 and darker blue colors indicating highly polymorphic positions with conservation scores of 4 and below.

931

932

Author Contributions: M.L., and K.d.G. prepared the ^{15}N - ^{13}C -labeled protein samples (sub-cloning, protein expression and purification). P.B. made the NMR resonance assignment of the four proteins in the study conditions. J.G. wrote scripts for protein sequence analysis and homology modeling. C.R. and A.P. supervised the project, conceived experiments and modeling, participated in the interpretation, and M.L., A.P., N.D., C.R., S.C., P.G. wrote the article. A.P. also contributed to the funding acquisition with P.G. and T.K. All authors have read and agreed to the published version of the manuscript.

Funding: This research project was funded by the ANR project MagMAX (ANR-18-CE20-0016-02), the European Research Council (ERC-2019-STG-852482-ii-MAX), and supported by French Infrastructure for Integrated Structural Biology (FRISBI) grant No. ANR-10-INSB-05.

Acknowledgements

We are grateful to Liisa Holm for feedback in implementing Dali. The authors are grateful to J. Maidment (CBS, Montpellier) for careful proof reading and language correction of our manuscript. We are grateful to Matthew Bowler and Didier Nurizzo at the European Synchrotron Radiation Facility (ESRF), Grenoble, France for providing assistance in using beamline ID30A-1. The authors gratefully acknowledge the ESRF for provision of synchrotron radiation facilities via Block Allocation Group beamtime.

Supporting information

S1 Fig. Template-based modeling of MAX effector sequences

S2 Fig. NMR structures and AF models

S3 Fig. Groups of AlphaFold models

S4 Fig. Singletons MAX effectors with structured extensions

S5 Fig. Hydrophobic residues on the surface of AVR-Pik and AVR-Pia

S6 Fig. Amino-acid polymorphism mapped on the surface of AF MAX models

S1 Table. List of *Pyricularia* (syn. *Magnaporthe*) *oryzae* entries in the 94 MAX effector orthogroup (OG) clusters

S2 Table. Representative sequences of the 94 MAX effector orthogroup clusters

S3 Table. Report on structural studies of 10 putative MAX effectors (OG proteins)

S4 Table. Refinement statistics of MAX effector NMR structures and AF model superimposition

S5 Table. Summary of AlphaFold2 modeling statistics and list of validated MAX effectors

S6 Table. $\beta 1\beta 4$ MSA

S7 Table. Structural features of 77 AF-modeled structures of validated MAX effector, statistics and conservation scores.

S8 Table. Comparizon of our selection of MAX effectors with previous modelisation studies

Supplementary Materials_and_Methods. Crystallographic structure determination of MoToxB

S1 File. Zipped folder of AF MAX models

S2 File. Zipped folder of AF MAX models surfaces

References

1. Lo Presti L, Lanver D, Schweizer G, Tanaka S, Liang L, Tollot M, et al. Fungal Effectors and Plant Susceptibility. *Annu Rev Plant Biol.* 2015;66: 513–545. doi:10.1146/annurev-arplant-043014-114623
2. Sperschneider J, Williams AH, Hane JK, Singh KB, Taylor JM. Evaluation of Secretion Prediction Highlights Differing Approaches Needed for Oomycete and Fungal Effectors. *Front Plant Sci.* 2015;6. doi:10.3389/fpls.2015.01168
3. Seong K, Krasileva KV. Computational Structural Genomics Unravels Common Folds and Novel Families in the Secretome of Fungal Phytopathogen *Magnaporthe oryzae*. *Mol Plant-Microbe Interactions®.* 2021;34: 1267–1280. doi:10.1094/MPMI-03-21-0071-R
4. Seong K, Krasileva KV. Prediction of effector protein structures from fungal phytopathogens enables evolutionary analyses. *Nat Microbiol.* 2023;8: 174–187. doi:10.1038/s41564-022-01287-6
5. Yan X, Tang B, Ryder LS, MacLean D, Were VM, Eseola Bisola A, et al. The transcriptional landscape of plant infection by the rice blast fungus *Magnaporthe oryzae* reveals distinct families of temporally co-regulated and structurally conserved effectors. *Plant Cell.* 2023;35: 1360–1385. doi:https://doi.org/10.1093/plcell/koad036
6. de Guillen K, Ortiz-Vallejo D, Gracy J, Fournier E, Kroj T, Padilla A. Structure Analysis Uncovers a Highly Diverse but Structurally Conserved Effector Family in Phytopathogenic Fungi. *PLOS Pathog.* 2015;11: e1005228.
7. Le Naour—Vernet M, Charriat F, Gracy J, Cros-Arteil S, Ravel S, Veillet F, et al. Adaptive evolution in virulence effectors of the rice blast fungus *Pyricularia oryzae*. Seidl MF, editor. *PLOS Pathog.* 2023;19: e1011294. doi:10.1371/journal.ppat.1011294
8. Maqbool A, Saitoh H, Franceschetti M, Stevenson CEM, Uemura A, Kanzaki H, et al. Structural basis of pathogen recognition by an integrated HMA domain in a plant NLR immune receptor. *eLife.* 2015;4: e08709.
9. De la Concepcion JC, Franceschetti M, Maqbool A, Saitoh H, Terauchi R, Kamoun S, et al. Polymorphic residues in rice NLRs expand binding and response to effectors of the blast pathogen. *Nat Plants.* 2018 [cited 10 Jul 2018]. doi:10.1038/s41477-018-0194-x
10. Maidment JHR, Franceschetti M, Maqbool A, Saitoh H, Jantasuriyarat C, Kamoun S, et al. Multiple variants of the fungal effector AVR-Pik bind the HMA domain of the rice protein OsHIPP19, providing a foundation to engineer plant defense. *J Biol Chem.* 2021;296: 100371. doi:10.1016/j.jbc.2021.100371
11. Zhang S, Wang L, Wu W, He L, Yang X, Pan Q. Function and evolution of *Magnaporthe oryzae* avirulence gene *AvrPib* responding to the rice blast resistance gene *Pib*. *Sci Rep.* 2015;5: 11642. doi:10.1038/srep11642
12. Oikawa K, Fujisaki K, Shimizu M, Takeda T, Saitoh H, Hirabuchi A, et al. The blast pathogen effector AVR-Pik binds and stabilizes rice heavy metal-associated (HMA) proteins to co-opt their function in immunity. *Plant Biology*; 2020 Dec. doi:10.1101/2020.12.01.406389
13. Park CH, Shirsekar G, Bellizzi M, Chen S, Songkumarn P, Xie X, et al. The E3 Ligase APIP10 Connects the Effector AvrPiz-t to the NLR Receptor Piz-t in Rice. Dinesh-Kumar SP, editor. *PLOS Pathog.* 2016;12: e1005529. doi:10.1371/journal.ppat.1005529
14. Bai P, Park C, Shirsekar G, Songkumarn P, Bellizzi M, Wang G. Role of lysine residues of the *Magnaporthe oryzae* effector AvrPiz-t in effector- and PAMP-triggered immunity. *Mol Plant Pathol.* 2019;20: 599–608. doi:10.1111/mpp.12779
15. Xu J, Zhang Y. How significant is a protein structure similarity with TM-score =

- 0.5? Bioinformatics. 2010;26: 889–895. doi:10.1093/bioinformatics/btq066
16. Jumper J, Evans R, Pritzel A, Green T, Figurnov M, Ronneberger O, et al. Highly accurate protein structure prediction with AlphaFold. *Nature*. 2021;596: 583–589. doi:10.1038/s41586-021-03819-2
17. Senior AW, Evans R, Jumper J, Kirkpatrick J, Sifre L, Green T, et al. Improved protein structure prediction using potentials from deep learning. *Nature*. 2020;577: 706–710. doi:10.1038/s41586-019-1923-7
18. Taylor WR. Residual colours: a proposal for aminochromography. *Protein Eng Des Sel*. 1997;10: 743–746. doi:10.1093/protein/10.7.743
19. Källberg M, Wang H, Wang S, Peng J, Wang Z, Lu H, et al. Template-based protein structure modeling using the RaptorX web server. *Nat Protoc*. 2012;7: 1511–1522. doi:10.1038/nprot.2012.085
20. Baek M, DiMaio F, Anishchenko I, Dauparas J, Ovchinnikov S, Lee GR, et al. Accurate prediction of protein structures and interactions using a three-track neural network. *Science*. 2021;373: 871–876. doi:10.1126/science.abj8754
21. Van Der Lee R, Buljan M, Lang B, Weatheritt RJ, Daughdrill GW, Dunker AK, et al. Classification of Intrinsically Disordered Regions and Proteins. *Chem Rev*. 2014;114: 6589–6631. doi:10.1021/cr400525m
22. Liu Y, Chen S, Wang X, Liu B. Identification of Intrinsically Disordered Proteins and Regions by Length-Dependent Predictors Based on Conditional Random Fields. *Mol Ther - Nucleic Acids*. 2019;17: 396–404. doi:10.1016/j.omtn.2019.06.004
23. Monzon AM, Necci M, Quaglia F, Walsh I, Zanotti G, Piovesan D, et al. Experimentally Determined Long Intrinsically Disordered Protein Regions Are Now Abundant in the Protein Data Bank. *Int J Mol Sci*. 2020;21: 4496. doi:10.3390/ijms21124496
24. Marín M, Uversky VN, Ott T. Intrinsic Disorder in Pathogen Effectors: Protein Flexibility as an Evolutionary Hallmark in a Molecular Arms Race. *Plant Cell*. 2013;25: 3153–3157. doi:10.1105/tpc.113.116319
25. Sun H, Zhu X, Li C, Ma Z, Han X, Luo Y, et al. Xanthomonas effector XopR hijacks host actin cytoskeleton via complex coacervation. *Nat Commun*. 2021;12: 4064. doi:10.1038/s41467-021-24375-3
26. Aparicio Chacón MV, Van Dingenen J, Goormachtig S. Characterization of Arbuscular Mycorrhizal Effector Proteins. *Int J Mol Sci*. 2023;24: 9125. doi:10.3390/ijms24119125
27. Jaswal R, Rajarammohan S, Dubey H, Kiran K, Rawal H, Sonah H, et al. Intrinsically Disordered Kiwellin Protein-Like Effectors Target Plant Chloroplasts and are Extensively Present in Rust Fungi. *Mol Biotechnol*. 2023. doi:https://doi.org/10.1007/s12033-023-00717-y
28. Walsh I, Martin AJM, Di Domenico T, Tosatto SCE. ESpritz: accurate and fast prediction of protein disorder. *Bioinformatics*. 2012;28: 503–509. doi:10.1093/bioinformatics/btr682
29. Holm L. DALI and the persistence of protein shape. *Protein Sci*. 2020;29: 128–140. doi:10.1002/pro.3749
30. Zhang Y, Skolnick J. TM-align: a protein structure alignment algorithm based on the TM-score. *Nucleic Acids Res*. 2005;33: 2302–2309. doi:10.1093/nar/gki524
31. Schweke H, Mucchielli M-H, Chevrollier N, Gosset S, Lopes A. SURFMAP: A Software for Mapping in Two Dimensions Protein Surface Features. *J Chem Inf Model*. 2022;62: 1595–1601. doi:10.1021/acs.jcim.1c01269
32. Giraldo MC, Valent B. Filamentous plant pathogen effectors in action. *Nat Rev*

- Microbiol. 2013;11: 800–814. doi:10.1038/nrmicro3119
33. Wang H, Chou C, Hsu K, Lee C, Wang AH -J. New paradigm of functional regulation by DNA mimic proteins: Recent updates. IUBMB Life. 2019;71: 539–548. doi:10.1002/iub.1992
34. Dennehy R, Duggan N, Dignam S, McCormack S, Dillon E, Molony J, et al. Protein with negative surface charge distribution, Bnr1, shows characteristics of a DNA-mimic protein and may be involved in the adaptation of *Burkholderia cenocepacia*. MicrobiologyOpen. 2022;11. doi:10.1002/mbo3.1264
35. Goldenberg NM, Steinberg BE. Surface Charge: A Key Determinant of Protein Localization and Function. Cancer Res. 2010;70: 1277–1280. doi:10.1158/0008-5472.CAN-09-2905
36. Guo L, Zhang Y, Ma M, Liu Q, Zhang Y, Peng Y, et al. Crystallization of the rice immune receptor RGA5A_S with the rice blast fungus effector AVR1-CO39 prepared *via* mixture and tandem strategies. Acta Crystallogr Sect F Struct Biol Commun. 2018;74: 262–267. doi:10.1107/S2053230X18003618
37. Varden FA, Saitoh H, Yoshino K, Franceschetti M, Kamoun S, Terauchi R, et al. Cross-reactivity of a rice NLR immune receptor to distinct effectors from the rice blast pathogen *Magnaporthe oryzae* provides partial disease resistance. J Biol Chem. 2019;294: 13006–13016. doi:10.1074/jbc.RA119.007730
38. Levy ED. A Simple Definition of Structural Regions in Proteins and Its Use in Analyzing Interface Evolution. J Mol Biol. 2010;403: 660–670. doi:10.1016/j.jmb.2010.09.028
39. Fiser A. Template-Based Protein Structure Modeling. In: Fenyő D, editor. Computational Biology. Totowa, NJ: Humana Press; 2010. pp. 73–94. doi:10.1007/978-1-60761-842-3_6
40. Rozano L, Mukuka YM, Hane JK, Mancera RL. Ab Initio Modelling of the Structure of ToxA-like and MAX Fungal Effector Proteins. Int J Mol Sci. 2023;24: 6262. doi:10.3390/ijms24076262
41. Radom F, Plückthun A, Paci E. Assessment of ab initio models of protein complexes by molecular dynamics. MacKerell A, editor. PLOS Comput Biol. 2018;14: e1006182. doi:10.1371/journal.pcbi.1006182
42. Mortuza SM, Zheng W, Zhang C, Li Y, Pearce R, Zhang Y. Improving fragment-based ab initio protein structure assembly using low-accuracy contact-map predictions. Nat Commun. 2021;12: 5011. doi:10.1038/s41467-021-25316-w
43. Sillitoe I, Dawson N, Lewis TE, Das S, Lees JG, Ashford P, et al. CATH: expanding the horizons of structure-based functional annotations for genome sequences. Nucleic Acids Res. 2019;47: D280–D284. doi:10.1093/nar/gky1097
44. Fox NK, Brenner SE, Chandonia J-M. SCOPe: Structural Classification of Proteins—extended, integrating SCOP and ASTRAL data and classification of new structures. Nucleic Acids Res. 2014;42: D304–D309. doi:10.1093/nar/gkt1240
45. Rocafort M, Bowen JK, Hassing B, Cox MP, McGreal B, de la Rosa S, et al. The *Venturia inaequalis* effector repertoire is dominated by expanded families with predicted structural similarity, but unrelated sequence, to avirulence proteins from other plant-pathogenic fungi. BMC Biol. 2022;20: 246. doi:10.1186/s12915-022-01442-9
46. Bondos SE, Dunker AK, Uversky VN. On the roles of intrinsically disordered proteins and regions in cell communication and signaling. Cell Commun Signal. 2021;19: 88, s12964-021-00774–3. doi:10.1186/s12964-021-00774-3
47. Zhao B, Kurgan L. Deep learning in prediction of intrinsic disorder in proteins.

- Comput Struct Biotechnol J. 2022;20: 1286–1294. doi:10.1016/j.csbj.2022.03.003
48. Yu DS, Outram MA, Smith A, McCombe CL, Khambalkar PB, Rima SA, et al. The structural repertoire of *Fusarium oxysporum* f. sp. *lycopersici* effectors revealed by experimental and computational studies. biorxiv; 2021 Dec. doi:10.1101/2021.12.14.472499
49. Varden FA. Structure/function studies of effectors from the potato late blight and rice blast pathogens. University of East Anglia. 2019. Available: https://ueaeprints.uea.ac.uk/id/eprint/70234/1/FAVarden_100085474_PhD_Feb2019.pdf
50. Dubois C, Herrada I, Barthe P, Roumestand C. Combining High-Pressure Perturbation with NMR Spectroscopy for a Structural and Dynamical Characterization of Protein Folding Pathways. Molecules. 2020;25: 5551. doi:10.3390/molecules25235551
51. Roche J, Dellarole M, Royer CA, Roumestand C. Exploring the Protein Folding Pathway with High-Pressure NMR: Steady-State and Kinetics Studies. In: Akasaka K, Matsuki H, editors. High Pressure Bioscience. Dordrecht: Springer Netherlands; 2015. pp. 261–278. Available: http://link.springer.com/10.1007/978-94-017-9918-8_13
52. Dubois C, Lahfa M, Pissarra J, de Guillen K, Barthe P, Kroj T, et al. Combining High-Pressure NMR and Geometrical Sampling to Obtain a Full Topological Description of Protein Folding Landscapes: Application to the Folding of Two MAX Effectors from *Magnaporthe oryzae*. Int J Mol Sci. 2022;23: 5461. doi:10.3390/ijms23105461
53. Lahfa M, Mouhand A, de Guillen K, Barthe P, Kroj T, Roumestand C. Does a Similar 3D Structure Mean a Similar Folding Pathway? The Presence of a C-Terminal α -Helical Extension in the 3D Structure of MAX60 Drastically Changes the Folding Pathway Described for Other MAX-Effectors from *Magnaporthe oryzae*. 2023.
54. Bryant P, Pozzati G, Elofsson A. Improved prediction of protein-protein interactions using AlphaFold2. Nat Commun. 2022;13: 1265. doi:10.1038/s41467-022-28865-w
55. Yu D, Chojnowski G, Rosenthal M, Kosinski J. AlphaPulldown—a python package for protein–protein interaction screens using AlphaFold-Multimer. Cowen L, editor. Bioinformatics. 2023;39: btac749. doi:10.1093/bioinformatics/btac749
56. Lahfa M, Padilla A, De Guillen K, Pissarra J, Raji M, Cesari S, et al. 1H, 13C, 15 N backbone and side-chain NMR assignments for three MAX effectors from *Magnaporthe oryzae*. Biomol NMR Assign. 2022;16: 305–309. doi:10.1007/s12104-022-10095-2
57. Güntert P. Automated NMR structure calculation with CYANA. Methods Mol Biol Clifton NJ. 2004;278: 353–378. doi:10.1385/1-59259-809-9:353
58. Güntert P, Buchner L. Combined automated NOE assignment and structure calculation with CYANA. J Biomol NMR. 2015 [cited 18 Apr 2015]. doi:10.1007/s10858-015-9924-9
59. Shen Y, Bax A. Protein Structural Information Derived from NMR Chemical Shift with the Neural Network Program TALOS-N. In: Cartwright H, editor. Artificial Neural Networks. New York, NY: Springer New York; 2015. pp. 17–32. doi:10.1007/978-1-4939-2239-0_2
60. Nederveen AJ, Doreleijers JF, Vranken W, Miller Z, Spronk CAEM, Nabuurs SB, et al. RECOORD: A recalculated coordinate database of 500+ proteins from the PDB using restraints from the BioMagResBank. Proteins Struct Funct Bioinforma. 2005;59: 662–672. doi:10.1002/prot.20408
61. Laskowski RA, MacArthur MW, Moss DS, Thornton JM. PROCHECK—a program to check the stereochemical quality of protein structures. : 283–291.
62. Koradi R, Billeter M, Wüthrich K. MOLMOL: A program for display and analysis of

- macromolecular structures. *J Mol Graph.* 1996;14: 51–55.
63. Webb B, Sali A. Protein Structure Modeling with MODELLER. *Methods Mol Biol.* 2020;2199: 239–255. doi:10.1007/978-1-0716-0892-0_14
64. Fu L, Niu B, Zhu Z, Wu S, Li W. CD-HIT: accelerated for clustering the next-generation sequencing data. *Bioinformatics.* 2012;28: 3150–3152. doi:10.1093/bioinformatics/bts565
65. Katoh K, Standley DM. MAFFT Multiple Sequence Alignment Software Version 7: Improvements in Performance and Usability. *Mol Biol Evol.* 2013;30: 772–780. doi:10.1093/molbev/mst010
66. Gracy J, Chiche L. PAT: a protein analysis toolkit for integrated biocomputing on the web. *Nucleic Acids Res.* 2005;33: W65–W71. doi:10.1093/nar/gki455
67. Sonnhammer EL, Hollich V. Scoredist: A simple and robust protein sequence distance estimator. *BMC Bioinformatics.* 2005;6: 108. doi:10.1186/1471-2105-6-108
68. Gonnet GH, Cohen MA, Brenner SA. Exhaustive Matching of the Entire Protein Sequence Database. *Science.* 1992;256: 1443–1445. doi:10.1126/science.1604319
69. Steinegger M, Soding J. MMseqs2 enables sensitive protein sequence searching for the analysis of massive data sets. *Nat Biotechnol.* 2017;35: 1026–1028. doi:10.1038/nbt.3988
70. Mirdita M, Steinegger M, Söding J. MMseqs2 desktop and local web server app for fast, interactive sequence searches. Hancock J, editor. *Bioinformatics.* 2019;35: 2856–2858. doi:10.1093/bioinformatics/bty1057
71. Mirdita M, Schütze K, Moriwaki Y, Heo L, Ovchinnikov S, Steinegger M. ColabFold: making protein folding accessible to all. *Nat Methods.* 2022;19: 679–682. doi:10.1038/s41592-022-01488-1
72. Edgar RC. MUSCLE: multiple sequence alignment with high accuracy and high throughput. *Nucleic Acids Res.* 2004;32: 1792–1797. doi:10.1093/nar/gkh340
73. Remmert M, Biegert A, Hauser A, Söding J. HHblits: lightning-fast iterative protein sequence searching by HMM-HMM alignment. *Nat Methods.* 2011;9: 173–175. doi:10.1038/nmeth.1818
74. Mariani V, Biasini M, Barbato A, Schwede T. IDDT: a local superposition-free score for comparing protein structures and models using distance difference tests. *Bioinformatics.* 2013;29: 2722–2728. doi:10.1093/bioinformatics/btt473
75. Holm L. Using Dali for Protein Structure Comparison. In: Gáspári Z, editor. *Structural Bioinformatics.* New York, NY: Springer US; 2020. pp. 29–42. doi:10.1007/978-1-0716-0270-6_3
76. Heinig M, Frishman D. STRIDE: a web server for secondary structure assignment from known atomic coordinates of proteins. *Nucleic Acids Res.* 2004;32: W500–W502. doi:10.1093/nar/gkh429
77. Lefort V, Desper R, Gascuel O. FastME 2.0: A Comprehensive, Accurate, and Fast Distance-Based Phylogeny Inference Program: Table 1. *Mol Biol Evol.* 2015;32: 2798–2800. doi:10.1093/molbev/msv150
78. Jurrus E, Engel D, Star K, Monson K, Brandi J, Felberg LE, et al. Improvements to the APBS biomolecular solvation software suite. *Protein Sci.* 2018;27: 112–128. doi:10.1002/pro.3280